ChemComm

FEATURE ARTICLE

View Article Online
View Journal | View Issue

Cite this: *Chem. Commun.*, 2020, **56**, 14553

Electrochemical non-enzymatic glucose sensors: recent progress and perspectives

Ming Wei,†[a] Yanxia Qiao,†[a] Haitao Zhao,[b] Jie Liang,[b] Tingshuai Li,[b] Yonglan Luo,[b] Siyu Lu,[c] Xifeng Shi,[d] Wenbo Lu *[a] and Xuping Sun *[b]

Received 19th August 2020,
Accepted 30th September 2020

DOI: 10.1039/d0cc05650b

rsc.li/chemcomm

The detection of glucose has important significance in clinical medicine and the food industry, especially in the diagnosis of diabetes. In recent years, electrochemical non-enzymatic glucose sensors have attracted intensive attention to detect the glucose level with great progress. In this review, we summarize a variety of non-enzymatic glucose sensor materials, including precious metals Pt, Au and their alloy metals, non-precious transition metals and their metal oxides, composites and other functional materials. Moreover, fundamental insights into the reaction mechanism and influencing factors of materials are given. Finally, this review discusses the perspectives and challenges of future developments in electrochemical non-enzymatic glucose detection.

[a] *Key Laboratory of Magnetic Molecules and Magnetic Information Materials (Ministry of Education), School of Chemistry and Material Science, Shanxi Normal University, Linfen 041004, Shanxi, China. E-mail: luwb@sxnu.edu.cn*
[b] *Institute of Fundamental and Frontier Sciences, University of Electronic Science and Technology of China, Chengdu 610054, Sichuan, China. E-mail: xpsun@uestc.edu.cn*
[c] *Green Catalysis Center and College of Chemistry, Zhengzhou University, Zhengzhou 450001, Henan, China*
[d] *College of Chemistry, Chemical Engineering and Materials Science, Shandong Normal University, Jinan 250014, Shandong, China*
† These authors contributed equally to this work.

Wenbo Lu

Wenbo Lu received his PhD degree in Southeast University (SEU), China in 2016. From 2019 to 2020, he worked as a visiting scholar at University of Electronic Science and Technology of China, China. Now, he is an associate professor at School of Chemical and Materials Science, Shanxi Normal University, China. He has published over 80 articles and book chapters related to nanomaterials and sensors. His research interests include the design and fabrication of functional materials for electrocatalysis, electroanalytical chemistry, sensors and immunosensors.

Xuping Sun

Xuping Sun received his PhD degree in Changchun Institute of Applied Chemistry (CIAC), Chinese Academy of Sciences in 2006. During 2006–2009, he carried out postdoctoral research at Konstanz University, University of Toronto, and Purdue University. In 2010, he started his independent research career as a full Professor at CIAC and then moved to Sichuan University in 2015. In 2018, he joined University of Electronic Science and Technology of China where he found the Research Center of Nanocatalysis & Sensing. He was recognized as a highly cited researcher (2018–2020) in both areas of chemistry and materials science by Clarivate Analytics. He published over 480 papers with total citations over 40000 and an h-index of 105. His research mainly focuses on rational design of functional nanostructures toward applications in electrochemistry for energy conversion and storage, sensing, and the environment.

1. Introduction

A sensor is a device that records physical, chemical or biological changes of a substance and converts them into measurable signals. In other words, the sensor can help researchers explore the composition and content of specific substances in the unknown world, just as humans can look at the colourful world with their eyes. A sensor is mainly composed of three parts: sensitive detector, transducer and signal processor. The sensitive detector mainly has a selective response to the specific analyte, the transducer generates the corresponding signal, and the signal processor collects, amplifies and presents the signal. An electrochemical sensor is a kind of sensor which outputs the changes generated by the target substance in the form of an electrical signal. Compared with other detection methods, electrochemical analysis does not require large analytical instruments, has fast response speed, high sensitivity and selectivity, and can be used for real-time monitoring of target analytes, and based on these advantages, electrochemical analysis is widely used in environmental detection, the food industry and biomedical fields.[1–5] In practical electrical analysis and detection, the standard three-electrode system is usually used.[6,7] The working electrode is generally made of metal, metal oxide and carbon. If the bare electrode is used directly in electrochemical experiments, the reactant molecules will be in direct contact with the electrode surface, which will limit the scope of its application. In order to enhance the selectivity of the electrode to the measured material, functional nanomaterials are generally used to modify the electrode to meet the requirements of analysis. After the target molecules are successfully identified on the electrode surface, electrochemical measurement techniques, such as cyclic voltammetry and square wave voltammetry, are used to obtain the corresponding electrochemical signals, so as to obtain the target analysis information such as concentration (Fig. 1).[8,9]

Glucose is one of the most widely distributed monosaccharides in nature. It is the main energy source in living cells and plays an important role in biology.[10,11] The physical and chemical properties of glucose have been extensively studied since the German chemist Margraves isolated it from beet roots in 1717.[10] The blood glucose concentration of normal people is maintained between 3.9 and 6.1 mmol L^{-1} in a fasting state.[12] Both hypoglycaemia and hyperglycaemia have adverse effects on people's health.[13–15] Hypoglycemia will make people feel hungry, palpated or even unconscious, while hyperglycemia increases the risk of diabetes to some extent. In addition, the determination of glucose content in fruits and vegetables is also one of the indexes to determine its quality, which can be used as a reference for their cultivation. From the above discussion, it can be seen that the accurate, rapid, simple and real-time measurement of glucose is of great significance to clinical diagnosis, the food industry and other industries.[16,17]

The elegant combination of electrochemical techniques and glucose determination brings new paths for glucose concentration determination. In previous literature reports, the electrochemical sensors for glucose are mainly divided into enzyme sensors and enzyme-free sensors.[18]

As the most widely studied sensor, the research direction of glucose enzyme-based sensors is moving from invasive to wearable (Fig. 2).[19] In terms of development history, glucose enzyme sensors have undergone three generations of development, mainly relying on glucose oxidoreductase enzymes to complete the detection purpose.[20,21] As the bioactive centre of glucose enzyme sensors, oxidoreductase enzymes are divided into two categories, glucose oxidase (GOx) and glucose dehydrogenases (GDHs), GDHs can be further classified according to their redox cofactors.[22] The first generation of enzyme sensors took oxygen as the electron acceptor, and the glucose concentration was determined by the consumption of oxygen and the release of hydrogen peroxide.[23] However, the first generation of sensors also demonstrates many disadvantages. For example, in addition to glucose, biomolecules such as urea may also be oxidized due to the high potential required in the test process. The experimental results are greatly affected by oxygen partial pressure or dissolved oxygen, and the high concentration of hydrogen peroxide produced by the reaction will cause the enzyme activity to decrease or inactivate. In order to overcome the shortcomings of the first generation of enzyme sensors, the second generation of enzyme sensors chose the chemically modified layer as the electron acceptor, and the reduction of working potential and the disappearance of hydrogen peroxide broadened the linear range of the sensor and extended the life of the sensor. The electron transfer process of the third-generation enzyme sensor is directly between the enzyme and the electrode. Considering that the active centre of the enzyme is inside the molecule and the enzyme is prone to deform on the electrode, the use of the third-generation enzyme sensor is limited, but the

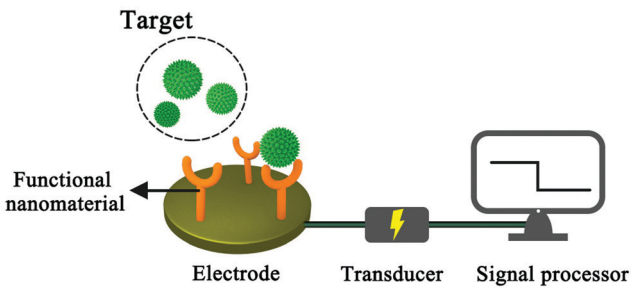

Fig. 1 Schematic diagram of an electrochemical sensor.

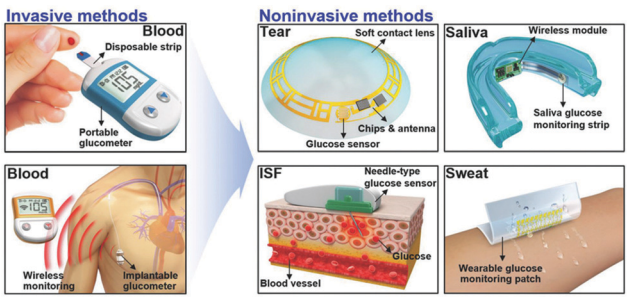

Fig. 2 The Schematic diagram of the research direction of glucose enzyme sensors from invasive to wearable. Reproduced ref. 19 with permission from Wiley-VCH Verlag GmbH & Co. KGaA, Weinheim, copyright 2018.

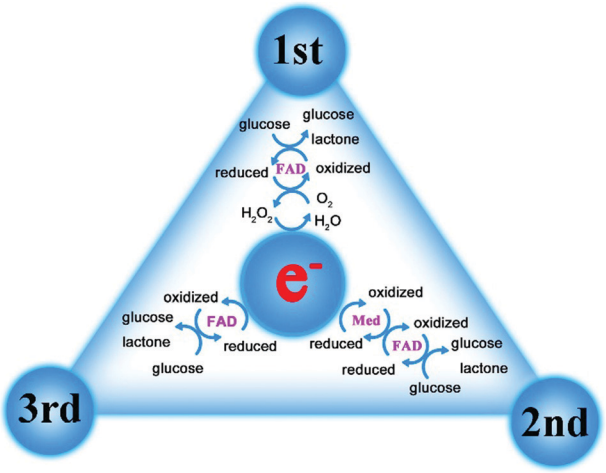

Fig. 3 The development of enzyme-containing sensors.

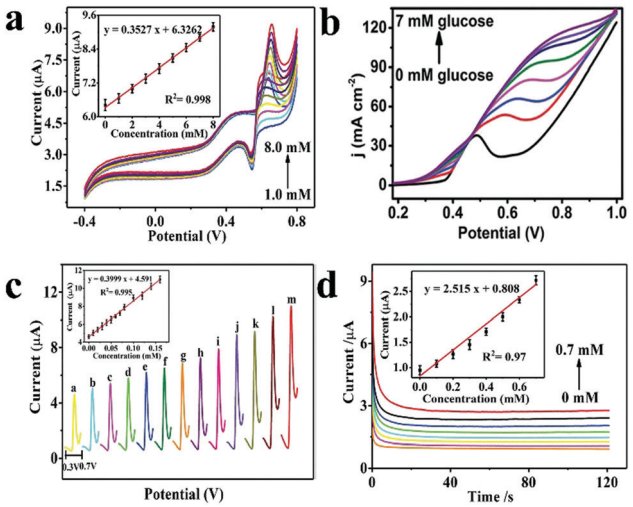

Fig. 4 (a) CV curves of the Ni–Fe hybrid nanocube/Nafion/GCE in 0.1 M NaOH containing various concentrations of glucose from 1.0 mM to 8.0 mM (scan rate at 50 mV s^{-1}).[24] (b) LSV curves for the Ni-MOF/NF in 0.1 M NaOH in the presence of varying glucose concentrations from 0 to 7 mM (scan rate at 30 mV s^{-1}).[25] (c) DPV curves of Ni–Fe nanocube/Nafion/GCE in 0.1 M NaOH with various glucose concentrations: 0, 0.1, 0.2, 0.3, 0.4, 0.5, 0.6, 0.7, 0.8, 1.0, 1.2, 1.4, and 1.6 mM, potential range: 0.3–0.7 V.[24] (d) Current–time curves at 0.63 V obtained for increasing glucose concentrations ranging from 0 mM to 0.7 mM in 0.1 M NaOH.[24] Reproduced from ref. 24 and 25 with permission from The Royal Society of Chemistry and the Centre National de la Recherche Scientifique, copyright 2019, 2018.

glucose oxidase can complete the electrocatalytic process on the appropriate electrode (Fig. 3). In order to further improve the performance of the glucose enzyme sensor, functional nanomaterials are introduced into the design of the enzyme sensor to further enhance the directional ability of the enzyme and amplify the conductive currents, especially in the introduction of noble metal nanoparticles such as Au and Pt.

The glucose enzyme sensor has high selectivity and sensitivity, but due to the existence of enzymes in its structure, it also has some defects. For example, the enzyme fixation step is complex, the exact amount of enzyme is difficult to ensure, and it is easily affected by temperature and pH. Therefore, glucose enzyme-free sensors have attracted more and more attention. Compared with enzyme sensors, non-enzyme sensors are easy to prepare, less affected by the surrounding environment, and can be stored for a long time. This review mainly gives a brief overview of the development of glucose non-enzyme sensors, especially in recent years, discusses the electrochemical measurement technology, reaction mechanism and influencing factors, and makes the development of a glucose non-enzyme sensor a certain prospect.

2. Electrochemical techniques

Electrochemical experiments are usually carried out by a three electrode system, which consists of a working electrode, reference electrode and auxiliary electrode. In the circuit, there are two loops, the current loop between the working electrode and the auxiliary electrode and the testing loop between the working electrode and the reference electrode.

The main variables in electrochemical measurement technology are potential, current, impedance and time, from which a series of electrochemical measurement methods are derived, such as cyclic voltammetry (CV), linear sweep voltammetry (LSV), differential pulse voltammetry (DPV), electrochemical impedance spectroscopy (EIS) and amperometric response methods, which greatly enriches the research methods of electrochemical sensors (Fig. 4).[24,25]

The CV method achieves the measurement of the electrochemical system by applying a triangular wave potential, which is the most basic electrochemical research method. It has been widely used in the study of the properties and mechanisms of electrochemical reactions and the kinetic parameters of electrode processes. The CV method can be used to judge the reversible degree of the electrode process and help researchers to explore the reaction mechanism. In the design of glucose non-enzyme sensors, the CV method is usually used to characterize the fabrication process of the sensor and explore the kinetic details of glucose catalysis at the working electrode. In addition, the CV method can be used to find the linear relationship between glucose concentration and electrochemical signal, which is a very widely used electrochemical technology.

The LSV method is a method to measure the corresponding polarization current at different potentials. The potential on the working electrode increases linearly with the scanning rate. However, compared with CV, the LSV method is less frequently used in glucose non-enzyme sensor related experiments. The LSV curve is a peak curve and can be described by Randles–Sevcik eqn (1) as follows:

$$i_p = 2.69 \times 10^5 n^{3/2} D^{1/2} \nu^{1/2} A c \quad (1)$$

The mechanism of the DPV method is to select the excitation signal as the sum of the pulse with a step potential or a linear potential and a fixed amplitude. The current is sampled twice before and after the pulse signal is used. The electrolytic current is obtained by subtracting the two currents. The DPV method is

suitable for trace analysis because of its low background current, high detection sensitivity and low detection limit. DPV technology is usually used to find the linear relationship of the sensor and is used frequently.

EIS measured the alternating current impedance of the electrode by controlling the alternating current potential of the electrode to make the alternating current change in accordance with the rule of sinusoidal wave with a small amplitude. Through EIS experiments, the resistance of the corresponding electrode can be obtained to determine its conductivity. EIS technology is mainly used to characterize the sensor assembly process, and the change of impedance is measured to indicate whether the functional nanomaterial successfully adheres to the electrode surface.

The amperometric response method is a control potential analysis method, by which the *i–t* curve of current variation with time is obtained. This method can be used to explore the dynamic reaction process of the electrode with high sensitivity. This electrochemical technique is frequently used in glucose sensor experiments, which can not only be used to find the linear relationship between glucose concentration and electrochemical signal, but also be used in anti-interference experiments.

3. Influencing factors of glucose non-enzyme sensors

On the premise of ensuring accuracy, in order to fully explore the performance of the sensor and seek a wider linear range, higher sensitivity and lower detection limit, the experimental conditions should be optimized during the assembly process of the sensor, including the pH of the supporting electrolyte, the amount of functional materials on the electrode and the scan rate.

3.1 The pH of the supporting electrolyte

The reaction of the analyte on the electrode usually involves H^+ and OH^-, that is, the pH of the supporting electrolyte will have a great influence on the electrochemical signal. The involvement of protons and electrons in the reaction process can be determined by using the Nernst equation to investigate the relationship between electric potential and pH. For example, when the slope is -58.5 mV pH^{-1}, it indicates that the number of protons involved is equal to the number of electrons.[26,27]

In the design of glucose non-enzyme sensors, the supporting electrolyte is usually NaOH solution with a concentration of 0.1 M, and in some reports, the concentration reached 0.5 M.[28–30] In addition, a few glucose non-enzyme sensors chose neutral PBS solution as the supporting electrolyte.[31,32] Due to the low glucose activity under acidic conditions, there are few reports about it.[33] The reason why glucose is easily catalysed by working electrodes under alkaline conditions has been explained by Sun *et al.* using density functional theory (DFT) calculations.[34] Sun *et al.* designed a glucose non-enzyme sensor based on cobalt phosphide (CoP) nanorods and calculated that glucose with OH^- was more likely to participate in the reaction than glucose solution. In the process of catalysis, electrode materials played a role in accelerating electron transfer and improving catalytic performance. Gluconic acid was produced by the transfer of OH^- from the CoP surface without any transition states, as shown in eqn (2):

$$\text{Glucose} + 2OH^- \rightarrow \text{gluconolactone} + 2H_2O + 2e^- \quad (2)$$

Physiological environment analysis is tremendously important for accurate detection of glucose. The pH of human blood is 7.3–7.5. A great deal of research has been focused on the detection of glucose under physiological pH conditions. Zhang's group reported a teamed boronate affinity-based molecular imprinting microelectrode module with active temperature regulation that was fabricated for blood glucose detection in a physiological environment.[35] Zang *et al.* present a novel copper nanowires/MOFs/graphene oxide nanocomposite for glucose detection in a neutral pH environment. The sensor exhibits a wide linear range (20–26.6 mM) and a low detection limit of 7 μM, which can be used for the analysis of glucose in human serum samples.[36] Mello *et al.* studied the electro-oxidation of glucose using cyclic voltammetry under physiological pH conditions (pH = 7) on low-index Pt single crystal surfaces. It is clearly seen that glucose electro-oxidation is strongly dependent of the electrode structure in terms of catalytic activity and reaction mechanism. The final outcome of glucose electro-oxidation is mainly associated with the production of cyclic carbonate on Pt(100) sites in neutral solution.[37] Ernst *et al.* reported the process of electrooxidation of glucose studied in a buffer solution with pH 7.5. It is observed that the rate determining step of the experiment may be the dehydrogenation of the C_1-atom adjacent to the hemiacetal OH-group and the primary oxidation product is gluconolactone.[38] Therefore, glucose detection under neutral pH is also accomplished.

Electrochemical detection of glucose in acid-supported electrolytes has not been reported. However, in the process of glucose photochemical detection, acidic medium is allowed. For example, in the process of glucose detection by Fe-PCN-224 photochemical detection, the electrolyte is an acetic acid buffer system with pH 3.5.[39]

3.2 Scan rate

The scan rate is closely related to the peak shape of the electrochemical signal. Generally, the peak strength of the electrochemical signal is positively correlated with the scan rate. In the CV curve, the details of electrode reaction kinetics can be obtained by seeking the linear relationship between sweep velocity and response current. If there is a linear relationship between the response current and the square root of the sweeping velocity, it demonstrates that a diffusion controlled redox reaction occurs on the electrode; if there is a linear relationship between the response current and the scan rate, then there is an adsorption controlled redox reaction on the electrode. In the design of glucose non-enzyme sensors, the scan rate is generally controlled below 100 mV s^{-1}, such as 50 mV s^{-1}.

3.3 Selectivity

The ultimate goal of an electrochemical glucose sensor is to be applied to clinical detection. It is well known that blood is a complex system consisting mainly of plasma and blood cells.

The plasma is mainly composed of water, small biological molecules and plasma proteins. Glucose is present in the plasma. Serum is a non-coagulable mixture formed by the removal of fibrinogen from plasma, retaining most of the components in the plasma, and can maintain blood viscosity, pH, and osmotic pressure. In addition to glucose, serum also includes inorganic salt ions, such as Na^+, K^+, Ca^{2+}, Cl^- *etc.*, small biotrophic molecules such as sugars, amino acids, and some cell metabolites. These substances should be fully considered as interferents in selective experiments with electrochemical glucose sensors.

In general, amperometric methods are usually used for selective experimentation. At the same time, CV and DPV technology have also been reported for the selectivity study. In the design of an experimental process, special attention should be paid to the selection of potential, the types and concentrations of interfering substances and the supporting electrolyte, which has a very important influence on the selective study. The chosen potential should have a strong catalytic effect on glucose, while no catalytic effect or little effect on the interferents. Generally, potential optimization should be carried out first before the selectivity study of an amperometric experiment. The interferents should contain the serum and compositions which simulate the real environment of the human blood. Meanwhile, the concentration of interferents is higher by several times that of glucose, so as to make the experimental results more convincing. The testing environment usually selects the optimized supporting electrolyte solution that has been selected for previous electrochemical tests.

Luo *et al.* constructed an electrochemical glucose sensor using Cu-MOF. The selectivity of an electrochemical sensor experiment by choosing sucrose, fructose, NaCl, ascorbic acid, uric acid, dopamine hydrochloride and L-cysteine as interferents. The experimental results show that an obvious current corresponding to the addition of glucose emerged and no obvious current change corresponding to the addition of the interferents, proving that the glucose sensor has a superior selectivity.[40] Xin *et al.* used porous flower-like Ni_5P_4 to construct an electrochemical glucose sensor. The selective experiment was conducted by selecting uric acid, ascorbic acid, and dopamine as interferents by DPV technology. The oxidation peak of glucose does not change after the addition of interferents, proving that the electrochemical sensor has good selectivity.[41] In addition, Janyasupab *et al.* investigated the selectivity of electrochemical glucose sensors based on bimetallic CoFe-nitrogen-doped graphene using CV technology.[42]

4. Non-enzyme electrochemical sensors

At present, a variety of glucose non-enzyme sensors have been developed, which is mainly due to the rapid development of the nano field. The synthesis strategy of multi-functional and multi-morphologic nanomaterials has been developed, enriching the field of nanotechnology and bringing infinite possibilities for electrochemical sensors. According to the present research progress, there are three methods for the material synthesis of non-enzyme electrochemical glucose sensors: (i) small size, porous precious metal materials such as nanotubes, nanoflowers and nanoclusters were synthesized by using nanotechnology; (ii) combining with other materials, such as metals, inorganic carbon materials, metal–organic frameworks materials, organic materials, *etc.*; (iii) the surface of the electrode or nanomaterial is modified to increase the roughness and thus add the electrochemical active site.

4.1 Types of materials involved in the electrochemical sensor

In the design of glucose sensors, there are many types of substances involved, such as metals and their compounds, inorganic carbon materials, conductive polymers, metal–organic frameworks (MOFs), *etc.* These materials, individually or in combination, construct the sensor's working electrode. These composite materials give full play to their own advantages in the construction of glucose non-enzyme sensors, thus improving the performance of non-enzyme sensors, such as wider linear range, higher sensitivity and lower detection limit.

4.1.1 Metal. Metal here refers to metal elements, metal oxides, metal hydroxides, metal nitrides, metal phosphates and alloys involved in sensor design. Based on the metal's good electrical and thermal conductivity, a series of glucose non-enzyme sensors have been developed. An alloy is a substance with metallic properties made of two or more metals in a given way. The relative content and grain size of each component will influence the properties of the final alloy. In the design of electrochemical sensors, the electrochemical properties of alloys have attracted much attention. This is a way to improve the performance of electrochemical sensors by changing their composition, which fully embodies the idea of combination. The reason why alloys can effectively improve their performance as electrocatalysts can be attributed to the synergistic catalytic effect of metals, and the biocompatibility of materials will also be improved with the participation of Au.[43] In the selection of alloy materials, elements filled with d orbitals and vacant orbitals are generally selected for combination.[44] The following discussion in this article will be based on the classification of metals.

4.1.2 Carbon materials. Carbon-based materials, including carbon dots, carbon nanotubes, carbon fibres, graphene, and fullerenes, have attracted more and more attention in recent years due to their unique physical and chemical properties.[45,46] Take graphene for example; it has high specific surface area, satisfactory chemical stability, excellent mechanical strength, outstanding electron transfer rate and remarkable biocompatibility, and in addition, it can be used to fix various substrate surfaces or edges which contain oxygen functional groups, such as hydroxyl, carboxyl and epoxy groups, and enhance the electrical conductivity of various materials. These advantages make carbon materials a candidate for catalytic materials for electrochemical sensors. Fig. 5 shows the composite material synthesized by Tang *et al.* using $NiCoO_2$ nanosheets and carbon nanotubes. Based on this material, the electrochemical sensor sensitivity was 1424.41 $\mu A\ cm^{-2}\ mM^{-1}$ and the detection limit was 1.14 μM.[47]

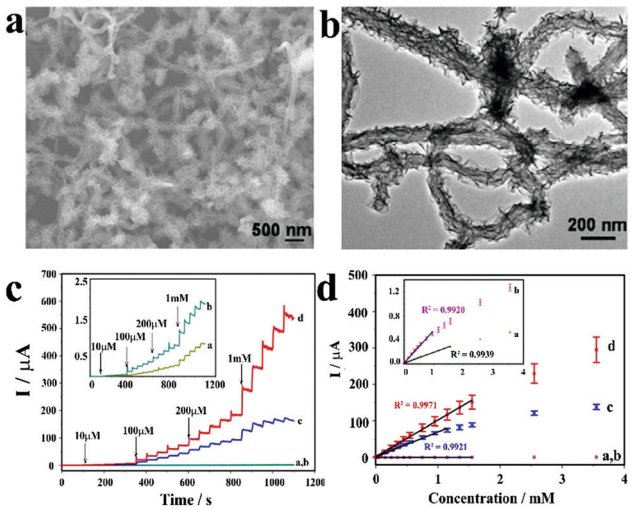

Fig. 5 (a) SEM image of $NiCoO_2$@CNT. (b) TEM image of $NiCoO_2$@CNT. (c) Amperometric responses to the successive additions of glucose. (d) The calibration curves obtained in the 0.1 M NaOH/NaAc buffer (pH 12.0). Reproduced ref. 47 with permission from Elsevier B.V., copyright 2015.

4.1.3 Conducting polymers. Conductive polymer material is a polymer material whose main chain has a conjugated principal electron system, which can reach the conductive state through doping, and the conductivity is above 1000 S cm^{-1}, including polypyrrole (PPy), polyaniline (PANI), poly-phenylene-vinylene (PPV), poly(3,4-ethylene dioxythiophene) (PEDOT), *etc.* Liu *et al.* synthesized a glucose electrocatalyst by combining CuO with PANI. The result indicates that the electrode exhibits a wide range of 0.001–19.899 mM, and low detection limit of 0.45 μM (Fig. 6).[48]

4.1.4 Metal–organic frameworks. Metal–organic frameworks (MOFs) are porous materials formed by self-assembly of organic ligands and metal ions or clusters through coordination bonds. MOF materials are various, with large porosity and specific surface area and adjustable pores, which can be applied in many fields such as energy storage and catalysis.[49–51] Li *et al.* prepared a working electrode with a Co-MOF loaded on nickel foam, with a sensor sensitivity of 10 886 μA cm^{-2} mM^{-1} and a detection limit as low as 1.3 nM (Fig. 7).[52]

From the above discussion, the construction of glucose non-enzyme sensors is based on the organic combination of various materials, which fully reflects the method of combination. Table 1 shows the performance of some glucose non-enzyme sensors based on metals, carbon materials, conductive polymers and MOFs.

4.2 Metal non-enzyme electrochemical sensors

With the exception of alkali metals, most metals are good conductors of heat and electricity. Due to the strength of the metal bond, the properties of different metals show great differences.

At present, precious metals represented by gold and platinum and transition metals represented by cobalt and nickel have been widely used in the design of glucose non-enzyme sensors.

4.2.1 Precious metal non-enzyme electrochemical glucose sensors. Precious metals mainly include gold (Au) and platinum (Pt) group metals, which have metallic lustre and stable properties.

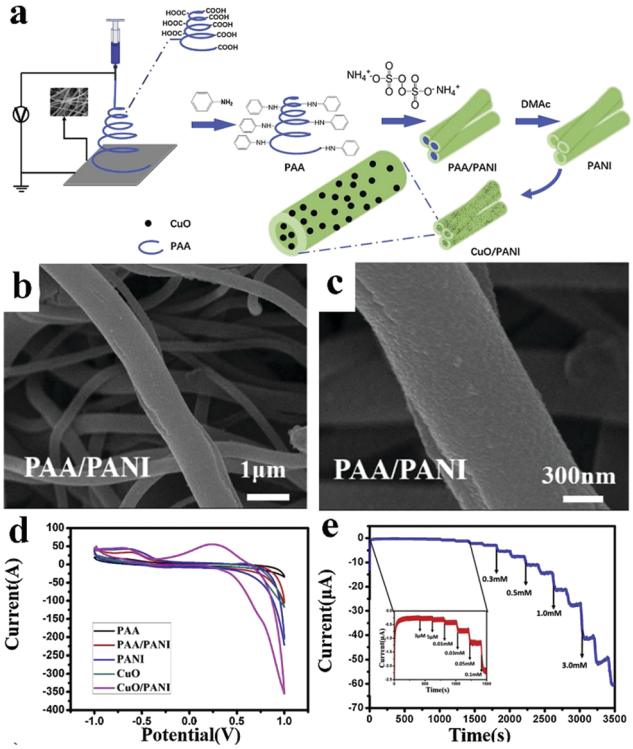

Fig. 6 (a) Schematic diagram of CuO/PANI nano-hybrid fiber synthesis. (b) Low magnification SEM image of the PAA hybrid nanofiber covered by PANI. (c) High magnification SEM image of the PAA hybrid nanofiber covered by PANI. (d) CV curves of GCEs modified with CuO/PANI nano-hybrid fibers. (e) Amperometric response of GCEs modified with CuO/PANI nano-hybrid fibers. Reproduced ref. 48 with permission from Elsevier B.V., copyright 2019.

Platinum and gold are widely used in the construction of glucose sensors due to their excellent electrochemical performance, sufficient stability and reproducibility. In order to improve the catalytic ability of noble metals to glucose, so as to achieve the best performance of the sensor, the synthesis of nano-sized, porous, rough surface precious metal materials has become a research hotspot.[77–80] Some nanostructures and the electrochemical performance of the glucose sensors are shown in Fig. 8.[77,80]

Platinum and gold can be used in many applications, such as monetary metal, jewellery, pharmaceuticals (such as gold nanoparticles for psoriasis treatment[81]), and chemical catalysts. Generally speaking, large bulks of gold and platinum will not be directly used in the catalytic process of the reaction, for many reasons. Taking platinum as an example, it has excellent catalytic ability for glucose in neutral solution, but it also has disadvantages, in the presence of chloride ions, platinum's ability to oxidize glucose is reduced; in addition, it is easily affected by uric acid and other interferents, and has a poor selectivity.[82] In order to overcome these disadvantages, various means are used to synthesize nanoscale small size precious metal materials to increase the specific surface area and roughness, which is one of the strategies to solve the problem. Yeast extract was introduced into the synthesis of Pt nanoparticles; it contains many biological molecules, such as amino acids and proteins,

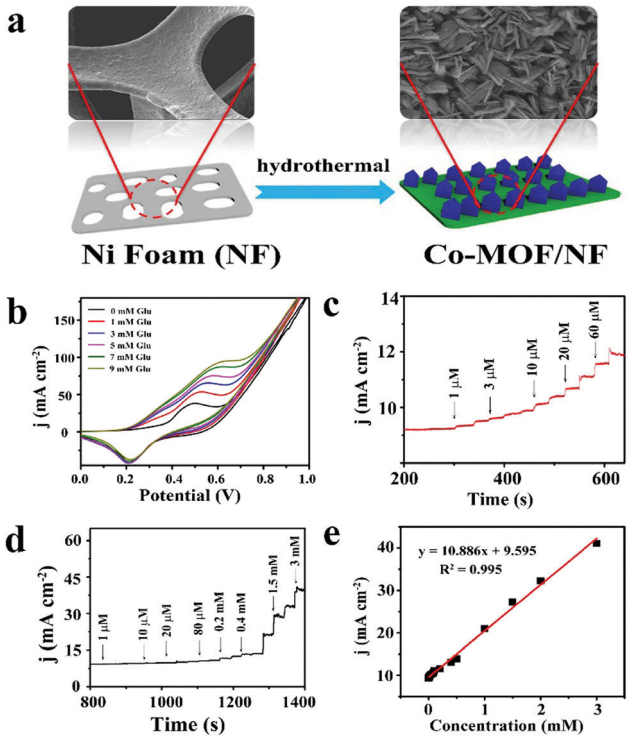

Fig. 7 (a) Schematic diagram of Co-MOF/NF synthesis. (b) CV curves of Co-MOF/NF in 0.1 M NaOH in the presence of various glucose concentrations. (c) and (d) The amperometric responses of Co-MOF/NF with successive addition of glucose in 0.1 M NaOH. (e) Calibration curve for the current response to different glucose concentrations. Reproduced ref. 52 with permission from Elsevier B.V., copyright 2018.

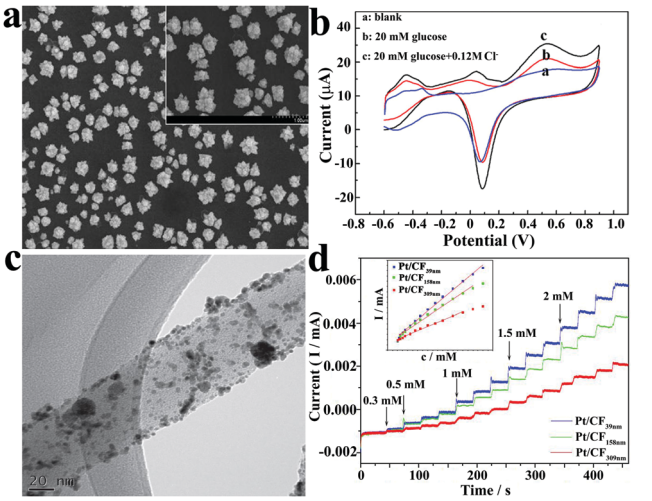

Fig. 8 (a) SEM image of Pt nanoflowers.[77] (b) CV curves of the Pt nanoflower electrode in 0.2 M neutral PBS.[77] (c) TEM image of the Pt nanoparticles on carbon fibers.[80] (d) Amperometric current–time response of Pt/CF in 0.1 M NaOH solution after the successive injection of different concentrations of glucose.[80] Reproduced ref. 77 and 80 with permission from Elsevier B.V., copyright 2011, 2015.

which provides enough sites for the reduction of H_2PtCl_6, and at the same time, the yeast extract can be used as a stabilizer, so it was selected as the template for the synthesis of Pt nanoclusters and enriched the preparation methods of noble metal nanomaterials.[83] Guo *et al.* electrodeposited platinum nanocrystals with an average diameter of 960 nm on a gold electrode using ultrasonic electrodeposition. In neutral medium, the non-enzyme

Table 1 The performances of composite and functional non-enzymatic glucose sensors

Electrode matrix	Sensitivity ($\mu A\ mM^{-1}\ cm^{-2}$)	Linear range (mM)	Detection limit (μM)	Electrolyte	Ref.
NiCoP/Ti	14 856	1–7	0.13	0.1 M NaOH	53
Ni–Co–S/TM	3291.5	0.001–3	0.12	0.1 M NaOH	54
Fe_3N–Co_2N/CC	4333.7	0.0001–1	0.077	0.1 M NaOH	55
NiO–CdO nanofiber	32.9	0–1.94	1.28	0.1 M NaOH	56
NiCo/$NiCoO_x$–FeOOH	7138	0.001–8	0.82	0.1 M NaOH	57
$CuCo_2O_4$ NWAs/CC	3930	0.001–0.93	0.5	0.1 M NaOH	58
CuTiPNPs	—	0.025–2	7	0.1 M NaOH	59
Cu NF@ AuNPs–GO NFs	—	0.001–0.1	0.018	0.1 M NaOH	60
amorphous Co–Ni hydroxid	11911.5	0.0025–5	0.127	0.5 M NaOH	61
NiCo–LDH/CC	5.12	0.001–1.5	0.12	0.1 M NaOH	62
Cu-BTC (MOFs)	943.3	0.0005–2.8	0.1	0.1 M NaOH	63
PAA-VS-PANI/GPL-FePc/GOx-CH	—	1–20	6.4	0.1 M PBS	64
g-C_3N_4	—	1–12	11	PBS (pH = 6.8)	65
GA@GNs/GNs	—	0.001–16	4×10^{-6}	0.1 M PBS	66
Pt/PANI/rGO/CuO	1252	0–13	1.5	0.1 M NaOH	67
Chitosan–polypyrrole	—	0.5–147	0.155	0.1 M PBS	68
Ni–Co–S/PPy/NF	—	0.002–0.14 0.14-2	0.82	0.1 M NaOH	69
APBA-PEI	—	0.5–50	2.5×10^{-5}	0.1 M NaOH	70
$NiP_{0.1}SnO_x$/PANI/	1625	0.01–1	0.13	0.1 M NaOH	71
CuO/cotton	1325	1–10			
$NiCo_2O_4$/PPy/NF	3059	0.001–20	0.22	0.1 M NaOH	72
Au-N-GQDs	—	1.0×10^{-5}–5×10^{-3}	3.3×10^{-3}	0.1 M NaOH	73
CPO-27-Ni^{II}	40.95	0.04–6	1.46	0.1 M NaOH	74
Ag@ZIF-67/GCE	0.379	0.002–1	0.66	0.1 M NaOH	75
Ni-MOF	14 845	0.04–2	0.085	0.1 M NaOH	25
Conductive Ni-MOF	21 744	0.001–8	0.66	0.1 M NaOH	76

sensor showed good catalytic performance for glucose with a sensitivity of 1.87 μA cm^{-2} mM^{-1}, linear range from 1 mM to 16 mM, and detection limit of 48 μM.[77]

In the process of glucose oxidation, Au has a low oxidation potential and a strong selectivity. Since its 3D orbitals are fully filled, Au also has a strong anti-interference ability; however, Au has low electrocatalytic capacity and high cost.[84] Zhong *et al.* creatively synthesized three-dimensional porous gold networks using an egg shell membrane as a template; this Au nanostructure has a very good catalytic effect on glucose, the electrochemical sensor using Au networks as the working electrode has good performance with the linear range 1.0–500 μM and 4.0–12 mM, and the detection limit is 0.2 μM (Fig. 9).[85] Shu *et al.* electrodeposited dendrite-like Au nanostructures on GCE, a non-enzyme sensor that also has superior performance.[86] In addition, platinum nanotubes, gold foam and other structures have also been used to design glucose non-enzyme sensors.[87–89] The reaction mechanism of platinum and gold catalysing glucose has been discussed in detail in related articles, and relevant details can be consulted.[90–92]

In addition to the elemental states discussed above, precious metals often appear in the form of alloys in the design of nonenzyme sensors. In terms of constituent elements, the alloy includes precious-precious metals, precious-other metals (metallic oxide) and in terms of the number of metals, the alloy combination includes bimetallic alloys and trimetallic alloys. Lin *et al.* constructed an electrochemical sensor by loading a PtAu alloy onto a GCE electrode. The presence of Au reduces the surface energy of Pt, which weakens the force between Pt and gluconolactone, thus increasing the stability of the catalyst based on the synergistic effect of the metals (Fig. 10).[93] Zhao *et al.* reached a similar conclusion in the construction of electrochemical sensors using PdCr alloy. Compared with single metal, the current density of the electrochemical sensors based on the PdCr alloy was greatly improved and could prevent Cl^- from deactivating the catalyst.[94] Jia *et al.* constructed an electrochemical sensor based on PtAu alloy on a GCE electrode. The performance of the sensor based on alloy material is greatly improved. With the increasing of Pt, the response current firstly increased and then

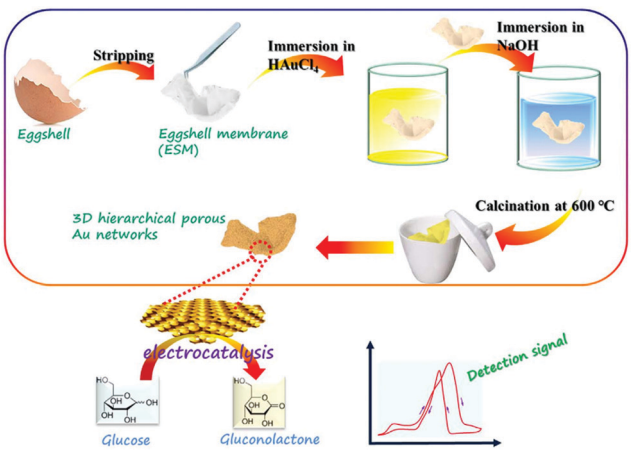

Fig. 9 Schematic diagram of 3D hierarchical porous Au network synthesis. Reproduced ref. 85 with permission from Elsevier B.V., copyright 2017.

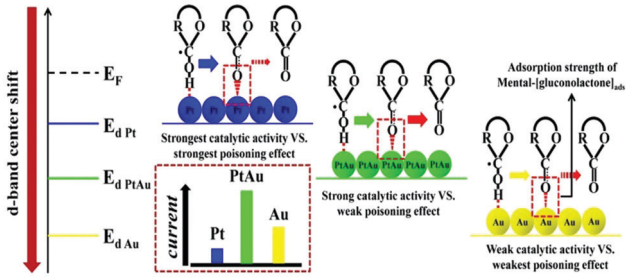

Fig. 10 Synergistic effect of PtAu alloy in the process of glucose oxidation. Reproduced ref. 93 with permission from Elsevier B.V., copyright 2020.

decreased, indicating that the proportion of metal in the alloy would affect the catalytic performance. This can be explained by the synergistic effect of the alloy and the change of catalytic sites.[95] Cao *et al.* also found that the bimetal PtCu alloys are superior in stability and catalytic efficiency due to electron coupling and ligand effects. PtCu alloy provides abundant activation sites for glucose oxidation, Pt atoms provide adsorption sites, and Cu atoms promote the formation of Cu-OR species, and can be used as electron donors.[96] In addition, synergies also exist in the study of electrochemical glucose sensors built by Au–Ni alloy, Au@Ag core nanorods, and Au–Ir alloy nanofibers.[97–99] Chakraborty *et al.* attached Au nanoparticles to CuO nanorods and demonstrated glucose sensitivity of 2009 μA mM^{-1} cm^{-2}, linear range of 5 μM to 1.325 mM, detection limit of 0.17 μM, and the synthesis schematic diagram and reaction mechanism are shown in Fig. 11.[100]

The combination of precious metals and carbon materials has become one of the trends in the design of glucose electrochemicalsensors, specifically, carbon-based materials generally exist as supports. Li *et al.* used PtPd nanoparticles loaded with ionic liquid functionalized reduced graphene to construct an electrochemical sensor. The corresponding time of the sensor was as low as 3 seconds, and the linear range was from 0.1 to 22 mM, with good repeatability, stability and selectivity.[101] Zhao *et al.* used electrodeposition to attach PtNi nanoparticles to multiwalled carbon nanotubes and systematically investigated the effect of Pt/Ni ratio on catalytic performance. The experimental results showed that when the ratio of Pt to Ni was 3 : 7, the electrochemical sensor had the best performance with the detection range of glucose up to 15 mM and the detection limit was 0.3 μM (Fig. 12).[102] In addition to the type and number of metals, the size of carbon material also affects the performance of the sensor. Ye *et al.* studied the influence of carbon fiber diameter on the performance of a Pt nanoparticle-based glucose sensor, and found that higher curvature and smaller diameter resulted in a greater number of Pt atoms on the surface, and the performance of the sensor is excellent with the linear range of 0.3–17 mM and the detection limit of 33 μM.[80] Nonenzymatic glucose sensors based on noble metals have been widely reported. The performance of some sensors is shown in Table 2.

4.2.2 Ni-Based, Cu-based and Co-based non-enzyme electrochemical glucose sensors. In addition to precious metals, transition metals are also widely used in the construction of glucose non-enzyme sensors, represented by Ni, Cu and Co and

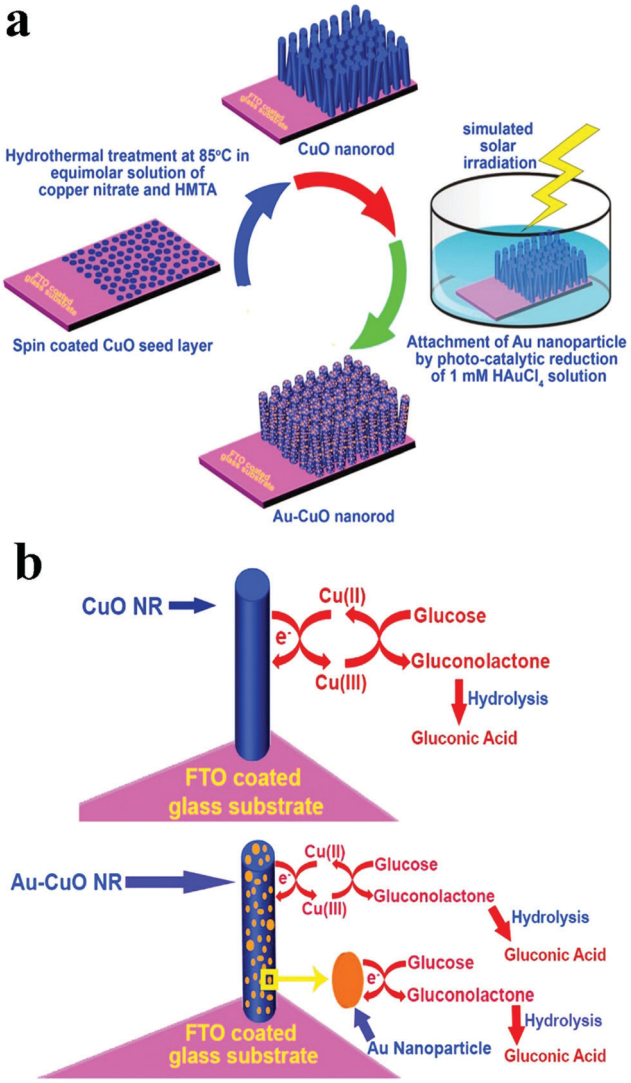

Fig. 11 (a) Schematic diagram of Au@CuO nanomaterial synthesis; (b) schematic representation of the glucose sensing mechanism. Reproduced from ref. 100 with permission from Elsevier B.V., copyright 2018.

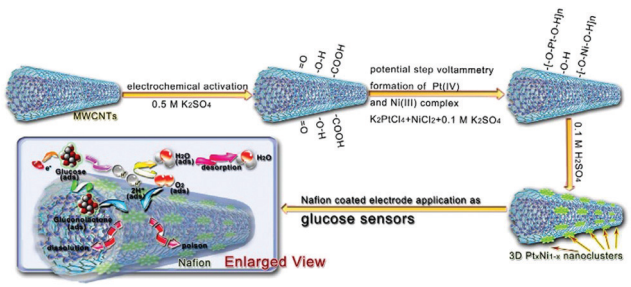

Fig. 12 Schematic diagram of the synthesis and reaction mechanism of the glucose sensor based on the flower-like 3D Pt_xNi_{1-x}/MWCNT catalysts. Reproduced ref. 102 with permission from Elsevier B.V., copyright 2016.

their compounds. Compared with precious metals, transition metals are abundant in nature and low in cost.[30]

As a common transition metal element, nickel is widely used in catalytic chemistry. Previous reports have demonstrated that nickel nanoparticles can be used in catalysis of organic reactions and can directly oxidize glucose in alkaline media.[131,132] However, nickel-based catalysts also have obvious disadvantages, such as poor electrical conductivity and mechanical strength, being easily affected by the external environment, and agglomeration occuring after a period of time.[133,134] Ni-based materials are widely used in glucose catalysis such as Ni, NiO, $Ni(OH)_2$, Ni_3N, Ni_2P, $Ni_3(PO_4)_2$, Ni-MOF and Ni alloys discussed above since Fleishman *et al.* demonstrated that Ni can partially electrooxidize organic matter under alkaline conditions.[135,136] The electrooxidation of glucose occurs on the surface of nickel-based materials, and electron transfer occurs between the Ni^{3+}/Ni^{2+} redox couple, regardless of the original form of nickel-based materials.[137] The mechanism of nickel-based material detecting glucose is shown in the following eqn (3)–(5):[138,139]

$$Ni + 2OH^- \rightarrow Ni(OH)_2 + 2e^- \quad (3)$$

$$Ni(OH)_2 + OH^- \rightarrow NiOOH + H_2O + e^- \quad (4)$$

$$NiOOH + glucose \rightarrow Ni(OH)_2 + glucolactone \quad (5)$$

Lu *et al.* directly used the commercial Ni foam (NF) as the working electrode to detect glucose. The linear range of the sensor was 0.05–7.35 mM, and the detection limit was 2.2 μM, which may be the simplest electrochemical glucose sensor based on Ni-based materials.[140] In the electrocatalytic process of glucose, Ni nanoparticles need the assistance of supports. For example, for graphene, Darvishi *et al.* used *Ab Initio* theoretical calculation and found that Ni element attached to the surface of graphene in the form of Ni_{13} nanoclusters to complete the catalysis of glucose.[133] In addition, silica nanochannel membrane as a support has also been reported.[141] Compared with nickel, NiO has higher stability and lower toxicity.[142] Guo *et al.* loaded NiO on NF and constructed an electrochemical glucose sensor with a linear range of 0.005 mM to 5.5 mm and a detection limit of 0.46 μM.[143] Similar to nickel foam, carbon nanosheets and carbon nanotubes can be used as supports in NiO electrochemical sensors, and the electrochemical glucose sensor based on $Ni(OH)_2$ is very similar to NiO.[29,135,144] In recent studies, nickel nitrides and phosphides have attracted attention due to their advantages in corrosion resistance and electron transfer, and these electrochemical sensors have shown excellent performance.[145–147] As a porous material, Ni-MOF is also used to detect glucose, and the pores in the material provide excellent adsorption sites for glucose.[74] The performance of some nickel-based glucose sensors is shown in Table 3.

Copper-based materials are also very popular catalytic materials for glucose due to their lower cost, non-toxicity and high electrochemical activity. Like nickel-based materials, copper-based materials can be used in many forms to electrically catalyse glucose. Metallic copper, CuO, Cu_2O, $Cu(OH)_2$, Cu_3N, CuS and Cu_3P participate in the reaction in various forms of morphological structures, such as nanorod, nanowire, nanoflower, nanoflake and nanocube. Considering high aspect ratio, metallic copper often appears in electrochemical glucose sensors in the form of nanowires. Zhang *et al.* used Cu nanowires to electrooxidize

Table 2 The performances of Pt/Au-based and alloy-based non-enzymatic glucose sensors

Electrode matrix	Sensitivity ($\mu A\ mM^{-1}\ cm^{-2}$)	Linear range (mM)	Detection limit (μM)	Electrolyte	Ref.
Pt nanotube arrays	0.1	2–14	1	0.1 M NaOH	88
Nanoporous Pt	642	0.1–1.5	—	0.1 M NaOH	103
Pt NFs	1.87	1–16	48	0.1 M NaOH	77
Pt-C NF	2.03	0.3–17	33	0.1 M NaOH	80
$Pt_{19.2}$/f-$CNF_{80.8}$ NF	22.7	0–10	0.42	0.1 M PBS	104
Pt film/Cu foam	9.62	1–11	385	0.1 M PB	105
Pt 3D dendritic	12.1	1–20	1.2	0.1 M NaOH	106
Pt nanoflower	11	1–7	—	0.1 M NaOH	107
PdCuPt NC	553	1–10	1.29	0.1 M NaOH	130
Pt-Pb NW	11.25	0–11	8	0.1 M PB	108
Pt NPs/CNTs	—	0.028–46.6	28	0.1 M NaOH	109
Pt–Cu nanochains	135	0.01–14	2.5	0.1 M NaOH	96
Pt Nps/graphene	6.36	0.01–12.55	1	0.1 M NaOH	110
Au foam	—	0.0005–12	0.14	0.3 M NaOH	89
Au-Co/GO	—	0.001–0.1	0.18	0.1 M PBS (pH = 7.4)	111
Au-CuO/FTO	2009	0.005–1.325	0.17	0.1 M NaOH	100
Au-NPs/ZnO-NRs	157.34	0.5–10	55	0.1 M NaOH	79
Au NPs/$Ni(OH)_2$ NS	82.71	0.002–6	0.66	0.1 M NaOH	112
Au@CuO NWs	4398.8	5×10^{-5}–5.9	0.5	0.1 M NaOH	113
Porous Au	11.8	2–10	5	0.1 M NaOH	114
Nanoporous Au film	66.0	1×10^{-5}–11	8.7	0.1 M NaOH	115
3D porous Au-graphene	5.2	0.1–2	25	0.1 M PBS, (pH = 7.4)	116
	4.56	2–16			
Macroporous Au–Pt	39.53	1–20	25	0.1 M NaOH	129
3DGFE	46.6	0.005–10	3.2	0.1 M NaOH	117
Au dendrite	190.7	0.1–25	50	0.1 M PB	86
GOD/AuNPs/rGO	—	0.005–0.9	0.08	0.2 M PBS (pH = 7.4)	118
Pt/Pb CNTs	17.8	Up to 11	1.8	10 mM PBS	119
PdCu alloy	—	1–30	1.9	0.1 M NaOH	120
PtCu flowers	—	0.01–2	0.1	PBS	78
Pt/Ni@rGO	171.92	0.002–5	6.3	0.1 M NaOH	121
Pt–Au alloy/Si substrate	352	0.006–11	6.0	0.1 M NaOH	122
Pt–Au/CD-R	0.25	1–33	5	0.1 M PB	123
PtAu/C	4.7	0–10	2	0.1 M PBS (pH = 7.4)	124
PtAu dendritic	31.2	0–7.5	—	0.1 M NaOH	125
Pt_2Pb NPs	—	0–10	—	0.1 M PBS (pH = 7.4)	126
PtAu/MWCNTs	10.7	0–24.44	10	0.1 M PBS (pH = 7.4)	127
Pd/Au cluster	75.3	0.1–30	50	0.1 M NaOH	128

Table 3 The performances of Ni-based non-enzymatic glucose sensors

Electrode matrix	Sensitivity ($\mu A\ mM^{-1}\ cm^{-2}$)	Linear range (mM)	Detection limit (μM)	Electrolyte	Ref.
Ni NP rGO/GCE	0.0025	0.00025–12	0.01	0.1 M NaOH	133
Ni 3D porous film	2900	0.0005–4	0.07	0.1 M NaOH	134
3D NiO/Ni foam	6658	0–5.5	0.46	0.1 M NaOH	143
NiO microfiber/FTO	1785.41	0.001–0.27	0.033	0.1 M NaOH	148
NiO-C/Ti foil	582.6	0–2.6	2	0.1 M NaOH	135
RGO-$Ni(OH)_2$/GCE	11.43	0.002–3.1	0.6	0.1 M NaOH	29
NiO-BP_2	2701	0.5–9	31	0.1 M NaOH	144
$NiCo_2O_4$/GCE	1917	0.01–0.3	0.6	0.2 M NaOH	149
Ni@SNM/FTO	62.3	0.01–12	0.44	0.1 M NaOH	141
Ni_3N/Ti	7688	0.2–1.5	0.06	0.1 M NaOH	145
$Ni_3(PO_4)_2$/CSs	219.898	0.005–2.5	1.67	0.1 M NaOH	150
	480.15	2.5–7.5			
Ni_2P NA/TM	7792	0.001–3	0.18	0.1 M NaOH	146
NiO nanosheets	838.09	0.0005–2.31	0.145	0.1 M NaOH	151
NiCPNP/rGO/GCE	—	0.01–8.75	0.14	0.1 M NaOH	152
Ni_5P_4/GCE	—	0.002–5.3	0.7	0.1 M NaOH	41
Ni/NC-800	660.3	0.002–4.658	0.12	0.1 M NaOH	153
$Ni(OH)_2/TiO_2$	192	0.03–14	8	0.1 M NaOH	154
3D porous Ni foam	—	0.05–7.35	2.2	0.1 M NaOH	140
Ni nanoflakes	7320	0.05–0.6	1.2	0.5 M NaOH	155

glucose, and the detection limit of the sensor was 35 nM with a sensitivity of 420.3 $\mu A\ mM^{-1}\ cm^{-2}$.[156] Na *et al.* prepared Cu nanowires by a hydrothermal method and further reduced the detection limit based on Cu nanowire sensors to 1 nM.[157] In order

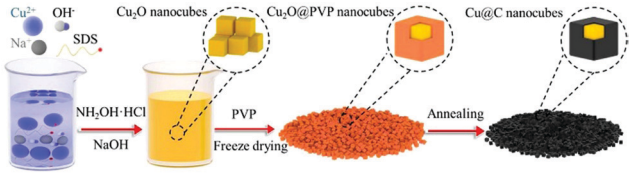

Fig. 13 Schematic diagram of well-aligned Cu@C core–shell nanocube synthesis. Reproduced from ref. 158 with permission from Elsevier B.V., copyright 2019.

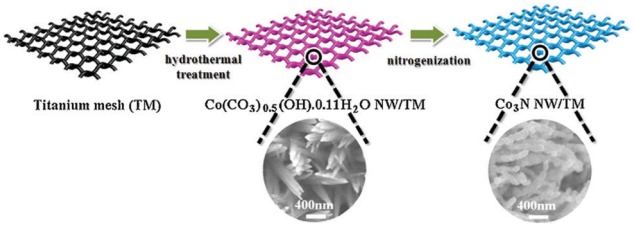

Fig. 14 Schematic diagram of Co_3N NW/TM synthesis. Reproduced ref. 180 with permission from Elsevier B.V., copyright 2017.

to further prevent Cu from being oxidized and improve the performance of glucose sensors, Ye *et al.* used a carbon shell wrapped around Cu cubes to form a core–shell structure to construct the sensor. The linear range of the sensor is 40 μM to 40 mM, with sensitivity of 2565 μA mM^{-1} cm^{-2} and detection limit of 21.35 μM (Fig. 13).[158] CuO is the most widely studied Cu-based material, and its catalytic glucose mechanism is similar to that of Ni, which is mainly completed by the Cu^{3+}/Cu^{2+} redox couple under alkaline conditions. The catalytic mechanism is shown below (6) and (7):[159]

$$CuO - OH^- \rightarrow CuOOH + e^- \quad (6)$$

$$CuOOH + glucose + e^- \rightarrow glucose + CuO + OH^- \quad (7)$$

CuO itself has poor conductivity and selectivity, when combined with precious metals or carbon materials, the sensor shows good catalytic performance for glucose.[113,160,161] In addition, Fu *et al.* and Sun *et al.* successfully synthesized copper sulfide, copper nitride and copper phosphide respectively and applied them to electrochemical detection of glucose. The sensor also showed excellent performance.[162–164] The performance of some Cu-based sensors is shown in Table 4.

As an environmentally friendly element, cobalt-based materials are also popular in the design of glucose non-enzyme sensors. Different from nickel and copper, cobalt has more valence states, so the reaction mechanism is slightly more complex. As shown in eqn (8) and (9), the mechanism of glucose electrocatalyzed by CoP is:[176]

$$CoOOH + OH^- \rightarrow CoO_2 + H_2O + e^- \quad (8)$$

$$CoO_2 + glucose + H_2O \rightarrow CoOOH + OH^- + gluconolactone \quad (9)$$

At present, a variety of cobalt-based materials including cobalt alloy, Co_3O_4, $Co(OH)_2$ and CoOOH are involved in the design of glucose sensors in various nanostructures.[177] Cobalt oxide, represented by Co_3O_4, is a standard semiconducting material that is biologically compatible but poorly conductive, so it is often combined with other materials, such as graphene, to form hybrids during the design of the cobalt based catalyst. Wang *et al.* synthesized the glucose electrocatalyst by loading the Co_3O_4 nanoclusters onto the three-dimensional Kenaf Stem-derived carbon (3D-KSCs), and the linear range of the sensor is 0.088 to 7 mM, and the detection limit is 26 μM.[178] Xiong *et al.* used the microplasma-based synthesis method to load Co(OH)F nanoflowers on the carbon cloth at room temperature and the sensor's sensitivity was 1806 μA mM^{-1} cm^{-2} and the detection limit was as low as 0.75 μM.[179] In addition to combining with other materials, the synthesis of new cobalt-based materials also attracted attention. Sun *et al.* successfully synthesized Co_3N and CoP, and further improved the performance of the sensor by utilizing the excellent conductive properties of transition metal nitride and phosphide (Fig. 14).[180] The sensitivity of glucose sensors based on Co_3N and CoP was 3325.6 μA mM^{-1} cm^{-2} and 5168.6 μA mM^{-1} cm^{-2}, and the detection limits were 1 μM and 0.5 μM, respectively.[176,180] The performance of some Co-based sensors is shown in Table 5.

4.2.3 Other metal non-enzyme electrochemical glucose sensors. In addition to the above-mentioned improved nickel,

Table 4 The performances of Cu-based non-enzymatic glucose sensors

Electrode matrix	Sensitivity (μA mM^{-1} cm^{-2})	Linear range (mM)	Detection limit (μM)	Electrolyte	Ref.
Cu-NW-CNT-BL	1907	0.01–2	0.0011	0.1 M NaOH	165
CuO nanotubes array	1890	0.005–3	0.1	1.0 M NaOH	166
$Cu_3(BTC)_2$–CuO nanorod	1523.5	1.2–5	1	0.1 M NaOH	167
$Cu/Cu(OH)_2$ NRA/CF	9180	0.001–1	0.45	0.1 M NaOH	168
CuNW_GSS	—	—	0.001	0.1 M NaOH	157
Cu_3N NA/CF	52.11	0.001–2	0.013	0.1 M NaOH	163
$Cu/CuO/Cu(OH)_2$	223.17	0–20	20	0.1 M NaOH	169
CuO/Cu_2O film	1950	0.1–6	1	0.1 M NaOH	170
CuO nanoflowers	2217	0–6	0.96	0.1 M NaOH	171
Cu@C core–shell nanocubes	2565	0.04–40	21.35	0.1 M NaOH	158
CuO NPs	—	0.005–2.3	0.5	0.1 M NaOH	172
Cu-RGO	50 400	0.002–2	0.5	0.1 M NaOH	173
$CuS-Cu_2S$	1923	0.001–2	0.33	0.1 M NaOH	164
Cu_2O/GNs	—	0.3 to 3.3	3300	0.1 M NaOH	174
Cu nanowires	420.3	0–3	35	0.1 M NaOH	156
Cu Nps/rGO	447.7	0–1.2	3.4	0.1 M NaOH	175

Table 5 The performances of Co-based non-enzymatic glucose sensors

Electrode matrix	Sensitivity ($\mu A\ mM^{-1}\ cm^{-2}$)	Linear range (mM)	Detection limit (μM)	Electrolyte	Ref.
$Co_3O_4/NiCo_2O_4$ DSNCs@G	304	0.01–3.52	0.384	0.1 M NaOH	181
Co_3O_4 bio-inspired pyrolytic carbon	1377	0.05–18	12	0.3 M NaOH	178
Co_3O_4/CuO NRA/CC	5405	0.001–0.5	0.38	0.1 M NaOH	182
Co_3O_4/Ni heterostructure	13855	0.04–3.6	1.0	0.1 M NaOH	183
Graphene–Co_3O_4 needle	—	0.05–0.3	<10	0.1 M NaOH	28
CoP nanowire/Ti mesh	5168.6	0.0005–1.5	0.1	0.1 M NaOH	176
Co_3N NW/TM	3325.6	0.001–2.5	0.05	0.1 M NaOH	180
CoO–Co–NC–rGO	3172	0.00005–0.01	0.34	0.1 M NaOH	184
Co_2N_x/NG	1167	0.01–4.75	6.93	0.1 M NaOH	185
CoSe/rGO	480	0–10	2.5	0.3 M NaOH	186
CoP NR	116.8	0.001–5.5	9	0.1 M NaOH	34
Co_3O_4 NW	300.8	0.005–0.57	5	0.1 M NaOH	187

Table 6 The performances of other metal-based enzyme-free glucose sensors

Electrode matrix	Sensitivity ($\mu A\ mM^{-1}\ cm^{-2}$)	Linear range (mM)	Detection limit (μM)	Electrolyte	Ref.
Zn–Sn/Cu	2135	0.0005–0.1	—	0.1 M NaOH	191
Mn-NiO	3212.52	0.002–0.67	0.8	0.1 M NaOH	189
ZnO–Cu–ZO	—	0.001–0.01	0.001	0.1 M NaOH	192
g-C_3N_4/α-Fe_2O_3	—	0.0025–0.58	0.58	0.1 M NaOH	193
CdS nanoribbon	1.436	0.002–0.225	0.08	0.1 M NaOH	194
MoS_2	570.71	0–30	—	0.1 M NaOH	31
$La_{0.6}Sr_{0.4}Co_{\delta 3}$/RGO	330	0.002–3.350	0.063	0.1 M NaOH	195
AgNPs–G	—	2–10	10	0.1 M NaOH	196
AgNPs/PANINFs	—	1–12	250	0.2 M PBS (pH = 7.4)	197
AgNPs	540.7	0.0286–9.8	5.5	0.1 M NaOH	198
α-MnO_2	3730	0.535-0.855	—	0.1 M NaOH	199
MnO_2 MWCNT	—	0.5–4.4	53	0.5 M NaOH	200
Co_7Fe_3/NPCSs	795.28	0.001-2.2	401.98	0.1 M NaOH	201
		2.2-14	1		
ZrO_2–Cu(I)	—	1–10	250	0.1 M NaOH	202
ZnO@C	2.97	0.1–10	—	0.1 M NaOH	203
Au–Ru nanocomposite/chitosan	240	0–6	1.7	0.1 M NaOH	204

copper and cobalt elements, other metals, such as Zn, Fe, Mo, Ag, Mn, *etc.* are also involved in the design of glucose non-enzyme sensors to some extent. Based on the chemical stability and good electron transport rate of ZnO, Raza *et al.* used Fe-doped ZnO (Fe-@ZnO) to complete the detection of glucose on the screen printed electrode and the detection limit was as low as 0.3 μM.[188] Previous study has confirmed that Mn can adjust the structure of the catalyst and increase the catalytic site. Gao and coworkers used Mn doping of NiO to construct an electrochemical sensor with the sensitivity of 3212.52 mA mM^{-1} cm^{-2} and the detection limit of 0.8 mM.[189] Similarly, considering that Li can enhance electrical conductivity and electron transfer rate, Luo *et al*. fabricated an electrochemical glucose sensor based on Li doping NiO with a detection limit as low as 0.1 mM.[190] The glucose sensor based on MoS_2 microflowers has a linear range of 0–30 mM, providing reference for the design of Mo-based material sensors.[31] Table 6 illustrates some other metal-based enzyme-free glucose sensors.

5. Introduction to other methods for glucose detection

In addition to immense amounts of research about nanomaterials, new methods and instruments have been developed to detect glucose in recent years, such as colorimetry,[205–208] optical methods,[209,210] surface plasmon resonance,[211] surface acoustic wave resonator (SAW),[212] paper-based analytical devices,[213] molecularly imprinted devices,[214] *etc.*

Luo *et al.* created a Surfac Acoustic Wave (SAW) glucose sensor based on Mn-doped ZnO multilayer structure. The experimental results confirmed that the sensitivity of the SAW glucose biosensor is 7.184 MHz mM^{-1} and the accuracy is 6.96×10^{-3} mM; in addition, the modified sensor has good stability and repeatability (Fig. 15a).[212] Karpova *et al.* proposed use of a flow-through glucose biosensor to monitor diabetes by continuous analysis immediately after excretion of undiluted sweat. Based on Prussian blue and glucose oxidase immobilized in perfluorosulfonated ionomer or gel of alkoxysilane, the sensor shows a high sensitivity with the latter reaching in batch mode 0.23 A M^{-1} cm^{-2}, and the detection range is from 0.001 to 1 mM (flow-through mode). Because the sensor records the dynamic glucose concentration of sweat in good agreement with the dynamic glucose level without any time delay, it thus offers broad prospects for monitoring blood glucose (Fig. 15b).[215] Wen and his colleagues constructed a signal-off photocopying biosensor based on polymer phenylethnylcopper (PPhECu). The sensor's linear range was 0.0005 to 5 mM, with a detection limit of 0.16 μM (Fig. 15c).[216]

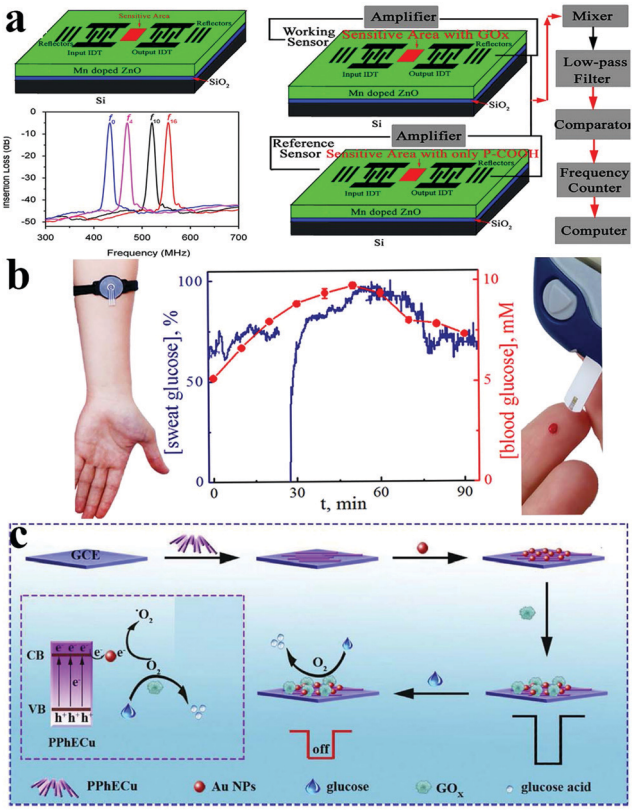

Fig. 15 (a) Schematic diagram of the glucose biosensor based on a Mn–ZnO/SiO_2/Si Love-mode SAW resonator and glucose biosensor measurement system.[212] (b) The used biosensors are based on Prussian Blue and glucose oxidase immobilized in perfluorosulfonated ionomer or gel of alkoxysilane.[215] (c) Synthesis and mechanism diagram of a glucose sensor based on PPhECu.[216] Reproduced ref. 212, 215 and 216 with permission from Elsevier B.V., American Chemical Society, Elsevier B.V., copyright 2013, 2019, 2019.

6. Summary and prospectives

In this review, we briefly summarize the development of non-enzymatic glucose sensors in recent years, and discuss the mechanisms and electrochemical techniques involved. The performance of glucose non-enzyme sensors is closely related to the selection of working electrode materials. Currently, there are mainly two approaches to improve the performance of enzyme-free glucose sensors: one is to increase the specific surface and electrochemical active sites by changing the topological structure of the material and the other is to form hybrids by doping or combining with other materials. With the continuous development of science and technology, many emerging materials, including nanodots, organic conductive materials and MOF materials, have been developed in the field of electrochemical analysis, further enriching the choice of electrocatalysts for glucose.

The blood glucose concentration of normal people is maintained between 3.9 mM and 6.1 mM in a fasting state. In the process of applying the experimental results to the clinic, the detection range of the electrochemical sensors should be selected first. If the linear range of the sensor is not within the physiological concentration, the actual sample needs to be diluted to the linear range in the actual detection. Soumabha *et al.* used $Ni_{60}Nb_{40}$ nanoglass to construct an electrochemical sensor with a linear range of 0.0001–10 mM.[217] Wu *et al.* fabricated a glucose sensor based on NiCo/$NiCoO_x$ hybrid nanoclusters with a linear range of 0.001–8 mM.[57] Yuan *et al.* constructed a sensor with the linear range of 2–14 mM using a platinum-nanotubule array.[88] Hu *et al.* built a glucose sensor based on platinum-replaced porous copper frameworks with a linear range of 1–11 mM.[105] Zang *et al.* presented a novel copper nanowires/MOFs/graphene oxide nanocomposite for glucose detection. The sensor exhibits a wide linear range (0.02–26.6 mM), which can be used for the analysis of glucose in human serum samples.[36] All of the above sensors can be used for glucose detection in the physiological concentration range, and are potential clinical candidates.

At present, common glucometers in the market are mainly divided into photochemical type and electrochemical type. Electrochemical type is mainly based on enzyme electrochemical glucose sensors. Glucose in the blood reacts with enzymes in the test paper, generating electrical signals that are converted by sensors into glucose concentrations. In the design of future glucometers, the combination of multiple technologies brings unlimited possibilities for blood glucose detection. Xu *et al.*

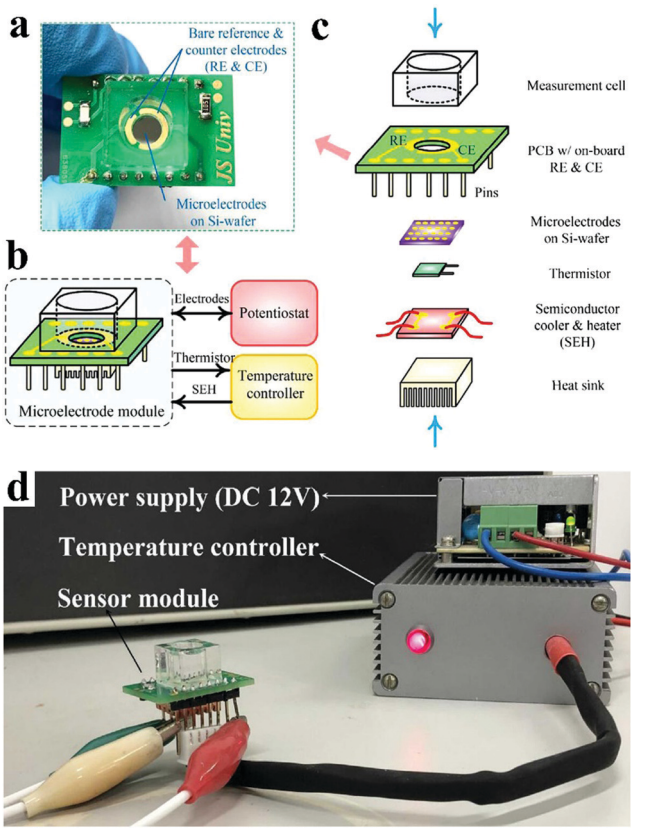

Fig. 16 (a) Optical photograph of the microelectrode module. (b) Typical application of the microelectrode module. (c) Structure of the microelectrode module. (d) Optical photograph of the microelectrode module under working conditions. Reproduced ref. 35 with permission from Elsevier B.V., copyright 2020.

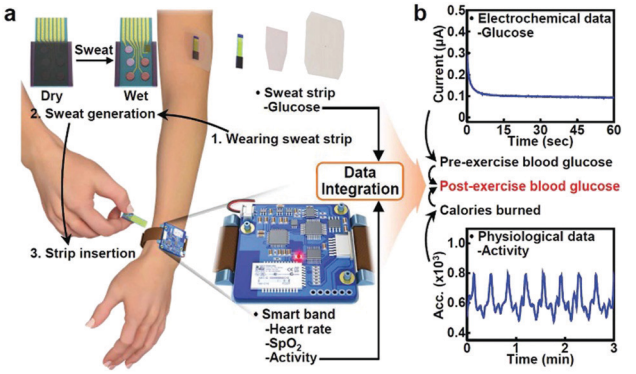

Fig. 17 (a) Schematic illustration of the wearable health monitoring system. (b) Schematic illustration showing combined use of electrochemical and physiological data. Reproduced from ref. 218 with permission from Wiley-VCH Verlag GmbH & Co. KGaA, Weinheim, copyright 2018.

developed a microelectrode module for the detection of blood glucose in a physiological environment (Fig. 16)[35] and Hong *et al.* developed a system that could analyze glucose levels in sweat and simultaneously monitor vital signs such as heart rate (Fig. 17).[218] Functional nanomaterials are expected to be used as sensing chips and the electrode of the glucometer. The glucometer will develop towards the direction of integration, miniaturization and wearability, so as to realize rapid, accurate, low-cost, real-time, noninvasive detection of glucose.

Conflicts of interest

There are no conflicts to declare.

Acknowledgements

This work was supported by the National Natural Science Foundation of China (No. 21575137 and 21705103), the Applied Basic Research Project of Shanxi Province (No. 201801D221392), the Graduate Education Innovation Project of Shanxi Province (2018SY057), the Graduate Education Innovation Project of Shanxi Normal University (2019XBY019), Collaborative Innovation Center for Shanxi Advanced Permanent Materials and Technology (2019-05), and the 1331 Engineering of Shanxi Province.

References

1 L. Zhang, J. Wang, F. Liu, Y. Xiong, Z. Liu, D. Jiang, Y. Li, D. Tu, Y. Wang and X. Pu, *RSC Adv.*, 2017, **7**, 12576–12585.
2 K. Li, W. Liu, Y. Ni, D. Li, D. Lin, Z. Su and G. Wei, *J. Mater. Chem. B*, 2017, **5**, 4811–4826.
3 M. Mohammadniaei, J. Yoon, T. Lee, B. G. Bharate, J. Jo, D. Lee and J.-W. Choi, *Small*, 2018, **14**, 1703970.
4 Y. Ya, C. W. Jiang, L. X. Mo, T. Li, L. P. Xie, J. He, L. Tang, D. J. Ning and F. Y. Yan, *Food Anal. Methods*, 2017, **10**, 1479–1487.
5 Y. Fu, Q. An, R. Ni, Y. Zhang, Y. Li and H. Ke, *Colloids Surf., A*, 2018, **559**, 289–296.
6 A. G. M. Ferrari, O. Amor-Gutierrez, E. Costa-Rama and M. T. Fernandez-Abedul, *Sens. Actuators, B*, 2017, **253**, 1207–1213.
7 J. Jin, J. Kim, J. Lee and N. Min, *Analyst*, 2011, **136**, 1910–1915.
8 Q. Niu, C. Bao, X. Cao, C. Liu, H. Wang and W. Lu, *Biosens. Bioelectron.*, 2019, **141**, 111445.
9 A. Pandikumar, G. T. Soon How, T. P. See, F. S. Omar, S. Jayabal, K. Z. Kamali, N. Yusoff, A. Jamil, R. Ramaraj, S. A. John, H. N. Lim and N. M. Huang, *RSC Adv.*, 2014, **4**, 63296–63323.
10 A. L. Galant, R. C. Kaufman and J. D. Wilson, *Food Chem.*, 2015, **188**, 149–160.
11 E. Wiercigroch, E. Szafraniec, K. Czamara, M. Z. Pacia, K. Majzner, K. Kochan, A. Kaczor, M. Baranska and K. Malek, *Spectrochim. Acta, Part A*, 2017, **185**, 317–335.
12 M. Sud, X. Wang, P. C. Austin, L. L. Lipscombe, G. E. Newton, J. V. Tu, R. S. Vasan and D. S. Lee, *Eur. Heart J.*, 2015, **36**, 924–931.
13 S. A. Amiel, B. M. Frier, S. R. Heller, R. J. McCrimmon, K. Khunti, P. Aschner, B. Childs, P. E. Cryer, L. Gonder-Frederick, E. R. Seaquist, B. E. de Galan, T. Jones, S. Zoungas, L. A. Leiter, Y. Y. Luo, U. Pedersen-Bjergaard and G. , The Int Hypoglycaemia Study, *Lancet Diabetes Endocrinol.*, 2019, **7**, 385–396.
14 L. Heinemann, G. Freckmann, D. Ehrmann, G. Faber-Heinemann, S. Guerra, D. Waldenmaier and N. Hermanns, *Lancet*, 2018, **391**, 1367–1377.
15 J. B. Buse, D. J. Wexler, A. Tsapas, P. Rossing, G. Mingrone, C. Mathieu, D. A. D'Alessio and M. J. Davies, *Diabetologia*, 2020, **63**, 221–228.
16 D. Papandreou, E. Magriplis, M. Abboud, Z. Taha, E. Karavolia, C. Karavolias and A. Zampelas, *Nutrients*, 2019, **11**, 2171.
17 P. Mirmiran, S. Hosseinpour-Niazi, L. Moghaddam-Banaem, M. Lamyian, A. Goshtasebi and F. Azizi, *Int. J. Vitam. Nutr. Res.*, 2019, **89**, 37–44.
18 H. Wang and A. R. Lee, *J. Food Drug Anal.*, 2015, **23**, 191–200.
19 H. Lee, Y. J. Hong, S. Baik, T. Hyeon and D. H. Kim, *Adv. Healthcare Mater.*, 2018, **7**, 1701150.
20 S. Ferri, K. Kojima and K. Sode, *J. Diabetes Sci. Technol.*, 2011, **5**, 1068–1076.
21 J. Wang, *Chem. Rev.*, 2008, **108**, 814–825.
22 J. Okuda-Shimazaki, H. Yoshida and K. Sode, *Bioelectrochemistry*, 2020, **132**, 107414.
23 L. C. Clark Jr. and C. Lyons, *Ann. N. Y. Acad. Sci.*, 1962, **102**, 29–45.
24 C. Bao, Q. Niu, X. Cao, C. Liu, H. Wang and W. Lu, *New J. Chem.*, 2019, **43**, 11135–11140.
25 W. Lu and X. Wu, *New J. Chem.*, 2018, **42**, 3180–3183.
26 W. Sun, M. Xi, L. Zhang, T. Zhan, H. Gao and K. Jiao, *Electrochim. Acta*, 2010, **56**, 222–226.
27 P. Wu, Q. Shao, Y. Hu, J. Jin, Y. Yin, H. Zhang and C. Cai, *Electrochim. Acta*, 2010, **55**, 8606–8614.
28 X. Wang, X. Dong, Y. Wen, C. Li, Q. Xiong and P. Chen, *Chem. Commun.*, 2012, **48**, 6490–6492.
29 Y. Zhang, F. Xu, Y. Sun, Y. Shi, Z. Wen and Z. Li, *J. Mater. Chem.*, 2011, **21**, 16949–16954.
30 T. Zhe, X. Sun, Y. Liu, Q. Wang, F. Li, T. Bu, P. Jia, Q. Lu, J. Wang and L. Wang, *Microchem. J.*, 2019, **151**, 104197.
31 Y. Zhai, J. Li, X. Chu, M. Xu, F. Jin, X. Li, X. Fang, Z. Wei and X. Wang, *J. Alloys Compd.*, 2016, **672**, 600–608.
32 Y.-L. T. Ngo, W. M. Choi, J. S. Chung and S. H. Hur, *Sens. Actuators, B*, 2019, **282**, 36–44.
33 F. Largeaud, K. B. Kokoh, B. Beden and C. Lamy, *J. Electroanal. Chem.*, 1995, **397**, 261–269.
34 Q. Sun, M. Wang, S.-J. Bao, Y. C. Wang and S. Gu, *Analyst*, 2016, **141**, 256–260.
35 X. Xu, C. Liu, W. Zhang and X. Zou, *Sens. Actuators, B*, 2020, **324**, 128720.
36 G. Zang, W. Hao, X. Li, S. Huang, J. Gan, Z. Luo and Y. Zhang, *Electrochim. Acta*, 2018, **277**, 176–184.
37 G. A. B. Mello, W. Cheuquepán and J. M. Feliu, *J. Electroanal. Chem.*, 2020, **878**, 114549.
38 S. Ernst, J. Heitbaum and C. H. Hamann, *J. Electroanal. Chem. Interfacial Electrochem.*, 1979, **100**, 173–183.
39 T. Li, P. Hu, J. Li, P. Huang, W. Tong and C. Gao, *Colloids Surf., A*, 2019, **577**, 456–463.
40 Y. Luo, Q. Wang, J. Li, F. Xu, L. Sun, Y. Bu, Y. Zou, H.-B. Kraatz and F. Rosei, *Inorg. Chem. Front.*, 2020, **7**, 1512–1525.
41 X. Xiao, Y. Wang, H. Cheng, Y. Cui, Y. Xu, T. Yang, D. Zhang and X. Xu, *Mater. Chem. Phys.*, 2020, **240**, 122202.
42 M. Janyasupab, C.-W. Liu, N. Chanlek, S. Chio-Srichan, C. Promptmas and W. Surareungchai, *Sens. Actuators, B*, 2019, **286**, 550–563.
43 C. Zhu, D. Du, A. Eychmüller and Y. Lin, *Chem. Rev.*, 2015, **115**, 8896–8943.
44 Y. Jiao, Y. Zheng, M. Jaroniec and S. Z. Qiao, *Chem. Soc. Rev.*, 2015, **44**, 2060–2086.

45 D.-W. Hwang, S. Lee, M. Seo and T. D. Chung, *Anal. Chim. Acta*, 2018, **1033**, 1–34.
46 S. K. Krishnan, E. Singh, P. Singh, M. Meyyappan and H. S. Nalwa, *RSC Adv.*, 2019, **9**, 8778–8881.
47 X. Tang, B. Zhang, C. Xiao, H. Zhou, X. Wang and D. He, *Sens. Actuators, B*, 2016, **222**, 232–239.
48 T. Liu, Y. Guo, Z. Zhang, Z. Miao, X. Zhang and Z. Su, *Sens. Actuators, B*, 2019, **286**, 370–376.
49 S. Kitagawa and R. Matsuda, *Coord. Chem. Rev.*, 2007, **251**, 2490–2509.
50 Q. Yang, Q. Xu and H. Jiang, *Chem. Soc. Rev.*, 2017, **46**, 4774–4808.
51 J. Zhou and B. Wang, *Chem. Soc. Rev.*, 2017, **46**, 6927–6945.
52 Y. Li, M. Xie, X. Zhang, Q. Liu, D. Lin, C. Xu, F. Xie and X. Sun, *Sens. Actuators, B*, 2019, **278**, 126–132.
53 Z. Wang, X. Cao, D. Liu, S. Hao, G. Du, A. M. Asiri and X. Sun, *Chem. Commun.*, 2016, **52**, 14438–14441.
54 X. Cao, K. Wang, G. Du, A. M. Asiri, Y. Ma, Q. Lu and X. Sun, *J. Mater. Chem. B*, 2016, **4**, 7540–7544.
55 D. Zhou, X. Cao, Z. Wang, S. Hao, X. Hou, F. Qu, G. Du, A. M. Asiri, C. Zheng and X. Sun, *Chem. – Eur. J.*, 2017, **23**, 5214–5218.
56 Y. Ding, Y. Wang, L. Zhang, H. Zhang and Y. Lei, *J. Mater. Chem.*, 2012, **22**, 980–986.
57 D. Wu, Z. Zou, X. Lu, K. Guo, N. Yang and C. Xu, *J. Mater. Sci.*, 2019, **54**, 10695–10704.
58 X. Luo, M. Huang, L. Bie, D. He, Y. Zhang and P. Jiang, *RSC Adv.*, 2017, **7**, 23093–23101.
59 D. Martín-Yerga, J. Carrasco-Rodríguez, J. L. G. Fierro, F. J. García Alonso and A. Costa-García, *Electrochim. Acta*, 2017, **229**, 102–111.
60 S. H. Baek, J. Roh, C. Y. Park, M. W. Kim, R. Shi, S. K. Kailasa and T. J. Park, *Mater. Sci. Eng., C*, 2020, **107**, 110273.
61 H. Li, L. Zhang, Y. Mao, C. Wen and P. Zhao, *Nanoscale Res. Lett.*, 2019, **14**, 135.
62 X. Wang, Y. Zheng, J. Yuan, J. Shen, J. Hu, A.-J. Wang, L. Wu and L. Niu, *Electrochim. Acta*, 2017, **224**, 628–635.
63 L. Li, Y. Liu, L. Ai and J. Jiang, *J. Ind. Eng. Chem.*, 2019, **70**, 330–337.
64 H. Al-Sagur, K. Shanmuga sundaram, E. N. Kaya, M. Durmuş, T. V. Basova and A. Hassan, *Biosens. Bioelectron.*, 2019, **139**, 111323.
65 J. Tian, Q. Liu, C. Ge, Z. Xing, A. M. Asiri, A. O. Al-Youbi and X. Sun, *Nanoscale*, 2013, **5**, 8921–8924.
66 R. Li, J. Zhang, Z. Li, J. Liu, Z. Gu and G. Wang, *Sens. Actuators, B*, 2015, **208**, 421–428.
67 L. Fang, Q. Zhu, Y. Cai, B. Liang and X. Ye, *J. Electroanal. Chem.*, 2019, **841**, 1–9.
68 Y. Fang, Y. Ni, G. Zhang, C. Mao, X. Huang and J. Shen, *Bioelectrochem.*, 2012, **88**, 1–7.
69 H. Dai, P. Cao, D. Chen, Y. Li, N. Wang, H. Ma and M. Lin, *Synth. Met.*, 2018, **235**, 97–102.
70 H. Çiftçi, E. Alver, F. Çelik, A. Ü. Metin and U. Tamer, *Microchim. Acta*, 2016, **183**, 1479–1486.
71 A. Sedighi, M. Montazer and S. Mazinani, *Biosens. Bioelectron.*, 2019, **135**, 192–199.
72 X. Duan, K. Liu, Y. Xu, M. Yuan, T. Gao and J. Wang, *Sens. Actuators, B*, 2019, **292**, 121–128.
73 P. Ran, J. Song, F. Mo, J. Wu, P. Liu and Y. Fu, *Microchim. Acta*, 2019, **186**, 276.
74 N. S. Lopa, M. M. Rahman, F. Ahmed, S. C. Sutradhar, T. Ryu and W. Kim, *J. Electroanal. Chem.*, 2018, **822**, 43–49.
75 W. Meng, Y. Wen, L. Dai, Z. He and L. Wang, *Sens. Actuators, B*, 2018, **260**, 852–860.
76 Y. Qiao, Q. Liu, S. Lu, G. Chen, S. Gao, W. Lu and X. Sun, *J. Mater. Chem. B*, 2020, **8**, 5411–5415.
77 M. Guo, H. Hong, X. Tang, H. Fang and X. Xu, *Electrochim. Acta*, 2012, **63**, 1–8.
78 H. Yang, Z. Wang, Q. Zhou, C. Xu and J. Hou, *Microchim. Acta*, 2019, **186**, 631.
79 P. Rattanawarinchai, N. Khemasiri, N. Soyeux, S. Jessadaluk, A. Klamchuen, S. Wirunchit, A. Rangkasikorn, N. Kayunkid, D. Phromyothin, S. Rahong and J. Nukeaw, *Jpn. J. Appl. Phys.*, 2019, **58**, SDDE04.
80 J. Ye, Z. Liu, C. Lai, C. Lo and C. Lee, *Chem. Eng. J.*, 2016, **283**, 304–312.
81 A. S. Thakor, J. Jokerst, C. Zavaleta, T. F. Massoud and S. S. Gambhir, *Nano Lett.*, 2011, **11**, 4029–4036.
82 G. Chang, H. Shu, Q. Huang, M. Oyama, K. Ji, X. Liu and Y. He, *Electrochim. Acta*, 2015, **157**, 149–157.
83 L. Jin, Z. Meng, Y. Zhang, S. Cai, Z. Zhang, C. Li, L. Shang and Y. Shen, *ACS Appl. Mater. Interfaces*, 2017, **9**, 10027–10033.
84 W. Zhao, R. Zhang, S. Xu, J. Cai, X. Zhu, Y. Zhu, W. Wei, X. Liu and J. Luo, *Biosens. Bioelectron.*, 2018, **100**, 497–503.
85 S. Zhong, J. Zhuang, D. Yang and D. Tang, *Biosens. Bioelectron.*, 2017, **96**, 26–32.
86 H. Shu, L. Cao, G. Chang, H. He, Y. Zhang and Y. He, *Electrochim. Acta*, 2014, **132**, 524–532.
87 K. Cai, Z. Lv, K. Chen, L. Huang, J. Wang, F. Shao, Y. Wang and H. Han, *Chem. Commun.*, 2013, **49**, 6024–6026.
88 J. Yuan, K. Wang and X. Xia, *Adv. Funct. Mater.*, 2005, **15**, 803–809.
89 N. Shen, H. Xu, W. Zhao, Y. Zhao and X. Zhang, *Sensors*, 2019, **19**, 1203.
90 M. W. Hsiao, *J. Electrochem. Soc.*, 1996, **143**, 759.
91 S. Park, H. Boo and T. D. Chung, *Anal. Chim. Acta*, 2006, **556**, 46–57.
92 M. Pasta, F. La Mantia and Y. Cui, *Electrochim. Acta*, 2010, **55**, 5561–5568.
93 L. Lin, S. Weng, Y. Zheng, X. Liu, S. Ying, F. Chen and D. You, *J. Electroanal. Chem.*, 2020, **865**, 114147.
94 D. Zhao, Z. Wang, J. Wang and C. Xu, *J. Mater. Chem. B*, 2014, **2**, 5195–5201.
95 H. Jia, G. Chang, M. Lei, H. He, X. Liu, H. Shu, T. Xia, J. Su and Y. He, *Appl. Surf. Sci.*, 2016, **384**, 58–64.
96 X. Cao, N. Wang, S. Jia and Y. Shao, *Anal. Chem.*, 2013, **85**, 5040–5046.
97 W.-C. Lee, K.-B. Kim, N. G. Gurudatt, K. K. Hussain, C. S. Choi, D.-S. Park and Y.-B. Shim, *Biosens. Bioelectron.*, 2019, **130**, 48–54.
98 H. L. Chia, C. C. Mayorga-Martinez, R. Gusmão, F. Novotny, R. D. Webster and M. Pumera, *Chem. Commun.*, 2020, **56**, 7909–7912.
99 A. Yu, S. Moon, T. Kwon, Y.-B. Cho, M. H. Kim, C. Lee and Y. Lee, *Sens. Actuators, B*, 2020, **310**, 127822.
100 P. Chakraborty, S. Dhar, K. Debnath, T. Majumder and S. P. Mondal, *Sens. Actuators, B*, 2019, **283**, 776–785.
101 M. Li, X. Bo, Y. Zhang, C. Han and L. Guo, *Biosens. Bioelectron.*, 2014, **56**, 223–230.
102 Y. Zhao, L. Fan, B. Hong, J. Ren, M. Zhang, Q. Que and J. Ji, *Sens. Actuators, B*, 2016, **231**, 800–810.
103 S. Joo, S. Park, T. D. Chung and H. C. Kim, *Anal. Sci.*, 2007, **23**, 277.
104 B. Singh, E. Dempsey, C. Dickinson and F. Laffir, *Analyst*, 2012, **137**, 1639–1648.
105 Y. Hu, X. Niu, H. Zhao, J. Tang and M. Lan, *Electrochim. Acta*, 2015, **165**, 383–389.
106 Q. Shen, L. Jiang, H. Zhang, Q. Min, W. Hou and J.-J. Zhu, *J. Phys. Chem. C*, 2008, **112**, 16385–16392.
107 S. Badhulika, R. K. Paul, Rajesh, T. Terse and A. Mulchandani, *Electroanalysis*, 2014, **26**, 103–108.
108 Y. Bai, Y. Sun and C. Sun, *Biosens. Bioelectron.*, 2008, **24**, 579–585.
109 G. Wei, F. Xu, Z. Li and K. D. Jandt, *J. Phys. Chem. C*, 2011, **115**, 11453–11460.
110 L. Meng, Y. Xia, W. Liu, L. Zhang, P. Zou and Y. Zhang, *Electrochim. Acta*, 2015, **152**, 330–337.
111 X. Qiao, X. Wei, Y. Hao, Y. Zhang, M. Xu and B. Ye, *Mater. Lett.*, 2019, **236**, 476–479.
112 J. Xu, T. Chen, X. Qiao, Q. Sheng, T. Yue and J. Zheng, *Colloids Surf., A*, 2019, **561**, 25–31.
113 A. K. Mishra, B. Mukherjee, A. Kumar, D. K. Jarwal, S. Ratan, C. Kumar and S. Jit, *RSC Adv.*, 2019, **9**, 1772–1781.
114 Y. Li, Y.-Y. Song, C. Yang and X.-H. Xia, *Electrochem. Commun.*, 2007, **9**, 981–988.
115 Y. Xia, W. Huang, J. Zheng, Z. Niu and Z. Li, *Biosens. Bioelectron.*, 2011, **26**, 3555–3561.
116 H. Shu, G. Chang, J. Su, L. Cao, Q. Huang, Y. Zhang, T. Xia and Y. He, *Sens. Actuators, B*, 2015, **220**, 331–339.
117 Y. Bai, W. Yang, Y. Sun and C. Sun, *Sens. Actuators, B*, 2008, **134**, 471–476.
118 X. Qin, Q. Li, A. M. Asiri, A. O. Al-Youbi and X. Sun, *Gold Bull.*, 2014, **47**, 3–8.
119 H. Cui, J. Ye, W. Zhang, C. Li, J. H. T. Luong and F. S. Sheu, *Anal. Chim. Acta*, 2007, **594**, 175–183.
120 H. Yang, Z. Wang, C. Li and C. Xu, *J. Colloid Interface Sci.*, 2017, **491**, 321–328.
121 R. Ayranci, B. Demirkan, B. Sen, A. Şavk, M. Ak and F. Şen, *Mater. Sci. Eng., C*, 2019, **99**, 951–956.
122 C. Li, H. Wang and Y. Yamauchi, *Chem. – Eur. J.*, 2013, **19**, 2242–2246.

123 N. Tavakkoli and S. Nasrollahi, *Aust. J. Chem.*, 2013, **66**, 1097–1104.
124 B. Singh, F. Laffir, T. McCormac and E. Dempsey, *Sens. Actuators, B*, 2010, **150**, 80–92.
125 K.-J. Chen, W.-N. Su, C.-J. Pan, S.-Y. Cheng, J. Rick, S.-H. Wang, C.-C. Liu, C.-C. Chang, Y.-W. Yang, C.-H. Wang and B.-J. Hwang, *J. Mater. Chem. B*, 2013, **1**, 5925–5932.
126 Y. Sun, H. Buck and T. E. Mallouk, *Anal. Chem.*, 2001, **73**, 1599–1604.
127 J. Ryu, K. Kim, H.-S. Kim, H. T. Hahn and D. Lashmore, *Biosens. Bioelectron.*, 2010, **26**, 602–607.
128 C. Shen, J. Su, X. Li, J. Luo and M. Yang, *Sens. Actuators, B*, 2015, **209**, 695–700.
129 Y.-J. Lee and J.-Y. Park, *Sens. Actuators, B*, 2011, **155**, 134–139.
130 S. Fu, C. Zhu, J. Song, M. Engelhard, H. Xia, D. Du and Y. Lin, *ACS Appl. Mater. Interfaces*, 2016, **8**, 22196–22200.
131 H. Ai, X. Huang, Z. Zhu, J. Liu, Q. Chi, Y. Li, Z. Li and X. Ji, *Biosens. Bioelectron.*, 2008, **24**, 1048–1052.
132 S. Bilal, W. Ullah and A.-U.-H. Ali Shah, *Electrochim. Acta*, 2018, **284**, 382–391.
133 S. Darvishi, M. Souissi, F. Karimzadeh, M. Kharaziha, R. Sahara and S. Ahadian, *Electrochim. Acta*, 2017, **240**, 388–398.
134 X. Niu, M. Lan, H. Zhao and C. Chen, *Anal. Chem.*, 2013, **85**, 3561–3569.
135 X. Li, A. Hu, J. Jiang, R. Ding, J. Liu and X. Huang, *J. Solid State Chem.*, 2011, **184**, 2738–2743.
136 M. Wang, D. He, M. Huang, X. Wang and P. Jiang, *J. Alloys Compd.*, 2019, **786**, 530–536.
137 Q. Wa, W. Xiong, R. Zhao, Z. He, Y. Chen and X. Wang, *ACS Appl. Nano Mater.*, 2019, **2**, 4427–4434.
138 H. Nie, Z. Yao, X. Zhou, Z. Yang and S. Huang, *Biosens. Bioelectron.*, 2011, **30**, 28–34.
139 Y. Mu, D. Jia, Y. He, Y. Miao and H.-L. Wu, *Biosens. Bioelectron.*, 2011, **26**, 2948–2952.
140 W. Lu, X. Qin, A. M. Asiri, A. O. Al-Youbi and X. Sun, *Analyst*, 2013, **138**, 417–420.
141 J. Ding, X. Li, L. Zhou, R. Yang, F. Yan and B. Su, *J. Mater. Chem. B*, 2020, **8**, 3616–3622.
142 C. Li, Y. Liu, L. Li, Z. Du, S. Xu, M. Zhang, X. Yin and T. Wang, *Talanta*, 2008, **77**, 455–459.
143 C. Guo, Y. Wang, Y. Zhao and C. Xu, *Anal. Methods*, 2013, **5**, 1644–1647.
144 T. Zhu, Y. Zhang, L. Luo and X. Zhao, *ACS Appl. Mater. Interfaces*, 2019, **11**, 10856–10861.
145 F. Xie, T. Liu, L. Xie, X. Sun and Y. Luo, *Sens. Actuators, B*, 2018, **255**, 2794–2799.
146 T. Chen, D. Liu, W. Lu, K. Wang, G. Du, A. M. Asiri and X. Sun, *Anal. Chem.*, 2016, **88**, 7885–7889.
147 Z. Ji, Y. Wang, Q. Yu, X. Shen, N. Li, H. Ma, J. Yang and J. Wang, *J. Colloid Interface Sci.*, 2017, **506**, 678–684.
148 F. Cao, S. Guo, H. Ma, D. Shan, S. Yang and J. Gong, *Biosens. Bioelectron.*, 2011, **26**, 2756–2760.
149 W. Huang, Y. Cao, Y. Chen, J. Peng, X. Lai and J. Tu, *Appl. Surf. Sci.*, 2017, **396**, 804–811.
150 T. Zhan, H. Yin, J. Zhu, J. Chen, J. Gong, L. Wang and Q. Nie, *J. Alloys Compd.*, 2019, **786**, 18–26.
151 M. Guo, L. Wei, Y. Qu, F. Zeng and C. Yuan, *Mater. Lett.*, 2018, **213**, 174–177.
152 W. Lu, X. Qin, A. M. Asiri, A. O. Al-Youbi and X. Sun, *Analyst*, 2013, **138**, 429–433.
153 W. Gao, Q. Li, M. Dou, Z. Zhang and F. Wang, *J. Mater. Chem. B*, 2018, **6**, 6781–6787.
154 A. Gao, X. Zhang, X. Peng, H. Wu, L. Bai, W. Jin, G. Wu, R. Hang and P. K. Chu, *Sens. Actuators, B*, 2016, **232**, 150–157.
155 Q. Yi, W. Huang, W. Yu, L. Li and X. Liu, *Electroanalysis*, 2008, **20**, 2016–2022.
156 Y. Zhang, L. Su, D. Manuzzi, H. V. E. de los Monteros, W. Jia, D. Huo, C. Hou and Y. Lei, *Biosens. Bioelectron.*, 2012, **31**, 426–432.
157 W. Na, J. Lee, J. Jun, W. Kim, Y. K. Kim and J. Jang, *J. Ind. Eng. Chem.*, 2019, **69**, 358–363.
158 J. Ye, D. Deng, Y. Wang, L. Luo, K. Qian, S. Cao and X. Feng, *Sens. Actuators, B*, 2020, **305**, 127473.
159 K. Tian, M. Prestgard and A. Tiwari, *Mater. Sci. Eng., C*, 2014, **41**, 100–118.
160 Z. Chen, B. Zhao, X.-Z. Fu, R. Sun and C.-P. Wong, *J. Electroanal. Chem.*, 2017, **807**, 220–227.
161 S. Pourbeyram, J. Abdollahpour and M. Soltanpour, *Mater. Sci. Eng., C*, 2019, **94**, 850–857.
162 L. Xie, A. M. Asiri and X. Sun, *Sens. Actuators, B*, 2017, **244**, 11–16.
163 Z. Wang, X. Cao, D. Liu, S. Hao, R. Kong, G. Du, A. M. Asiri and X. Sun, *Chem. – Eur. J.*, 2017, **23**, 4986–4989.
164 Y. Fu and W. Jin, *Mater. Sci. Eng., C*, 2019, **105**, 110120.
165 Y. P. Palve and N. Jha, *Mater. Chem. Phys.*, 2020, **240**, 122086.
166 L. Xu, Q. Yang, X. Liu, J. Liu and X. Sun, *RSC Adv.*, 2014, **4**, 1449–1455.
167 K. Kim, S. Kim, H. N. Lee, Y. M. Park, Y.-S. Bae and H.-J. Kim, *Appl. Surf. Sci.*, 2019, **479**, 720–726.
168 L. Bie, X. Luo, Q. He, D. He, Y. Liu and P. Jiang, *RSC Adv.*, 2016, **6**, 95740–95746.
169 P. Viswanathan, J. Park, D.-K. Kang and J.-D. Hong, *Colloids Surf., A*, 2019, **580**, 123689.
170 R. Li, X. Liu, H. Wang, Y. Wu, K. C. Chan and Z. Lu, *Electrochim. Acta*, 2019, **299**, 470–478.
171 C. Kong, J. Lv, X. Hu, N. Zhao, K. Liu, X. Zhang, G. Meng, Z. Yang and S. Yang, *Mater. Lett.*, 2018, **219**, 134–137.
172 S. Liu, J. Tian, L. Wang, X. Qin, Y. Zhang, Y. Luo, A. M. Asiri, A. O. Al-Youbi and X. Sun, *Catal. Sci. Technol.*, 2012, **2**, 813–817.
173 B. Wang, Y. Wu, Y. Chen, B. Weng and C. Li, *Sens. Actuators, B*, 2017, **238**, 802–808.
174 M. Liu, R. Liu and W. Chen, *Biosens. Bioelectron.*, 2013, **45**, 206–212.
175 Q. Wang, Q. Wang, M. Li, S. Szunerits and R. Boukherroub, *RSC Adv.*, 2015, **5**, 15861–15869.
176 Y. Liu, X. Cao, R. Kong, G. Du, A. M. Asiri, Q. Lu and X. Sun, *J. Mater. Chem. B*, 2017, **5**, 1901–1904.
177 M. Huang, X. Luo, D. He and P. Jiang, *Anal. Methods*, 2017, **9**, 5903–5909.
178 L. Wang, Y. Zhang, Y. Xie, J. Yu, H. Yang, L. Miao and Y. Song, *Appl. Surf. Sci.*, 2017, **402**, 47–52.
179 Q. Wang, Y. Chen, R. Zhu, M. Luo, Z. Zou, H. Yu, X. Jiang and X. Xiong, *Sens. Actuators, B*, 2020, **304**, 127282.
180 F. Xie, X. Cao, F. Qu, A. M. Asiri and X. Sun, *Sens. Actuators, B*, 2018, **255**, 1254–1261.
181 B. Xue, K. Li, L. Feng, J. Lu and L. Zhang, *Electrochim. Acta*, 2017, **239**, 36–44.
182 S. Cheng, S. DelaCruz, C. Chen, Z. Tang, T. Shi, C. Carraro and R. Maboudian, *Sens. Actuators, B*, 2019, **298**, 126860.
183 H. Xu, C. Xia, S. Wang, F. Han, M. K. Akbari, Z. Hai and S. Zhuiykov, *Sens. Actuators, B*, 2018, **267**, 93–103.
184 Y. Zhang, Y. Zhang, H. Zhu, S. Li, C. Jiang, R. J. Blue and Y. Su, *J. Alloys Compd.*, 2019, **780**, 98–106.
185 L. Kong, Z. Ren, S. Du, J. Wu and H. Fu, *Chem. Commun.*, 2014, **50**, 4921–4923.
186 M. C. D. Cooray, X. Zhang, Y. Zhang, S. J. Langford, A. M. Bond and J. Zhang, *J. Mater. Chem. A*, 2017, **5**, 19289–19296.
187 L. Kang, D. He, L. Bie and P. Jiang, *Sens. Actuators, B*, 2015, **220**, 888–894.
188 W. Raza and K. Ahmad, *Mater. Lett.*, 2018, **212**, 231–234.
189 J. Gao, T. Meng, S. Lu, X. Ma, Y. Zhang, D. Fu, Z. Lu and C. M. Li, *J. Electroanal. Chem.*, 2020, **863**, 114071.
190 X. Luo, Z. Zhang, Q. Wan, K. Wu and N. Yang, *Electrochem. Commun.*, 2015, **61**, 89–92.
191 S. Khan, M. A. Rasheed, A. Waheed, A. Shah, A. Mahmood, T. Ali, A. Nisar, M. Ahmad, S. Karim and G. Ali, *Mater. Sci. Semicond. Process.*, 2020, **109**, 104953.
192 A. Mahmoud, M. Echabaane, K. Omri, L. El Mir and R. Ben Chaabane, *J. Alloys Compd.*, 2019, **786**, 960–968.
193 L. Liu, J. Wang, C. Wang and G. Wang, *Appl. Surf. Sci.*, 2016, **390**, 303–310.
194 B. Saha, S. K. Jana, S. Majumder and S. Banerjee, *Sens. Actuators, B*, 2019, **283**, 116–123.
195 J. He, J. Sunarso, Y. Zhu, Y. Zhong, J. Miao, W. Zhou and Z. Shao, *Sens. Actuators, B*, 2017, **244**, 482–491.
196 Y. Zhang, S. Liu, L. Wang, X. Qin, J. Tian, W. Lu, G. Chang and X. Sun, *RSC Adv.*, 2012, **2**, 538–545.
197 G. Chang, Y. Luo, W. Lu, X. Qin, A. M. Asiri, A. O. Al-Youbi and X. Sun, *Catal. Sci. Technol.*, 2012, **2**, 800–806.
198 M. Ghiaci, M. Tghizadeh, A. A. Ensafi, N. Zandi-Atashbar and B. Rezaei, *J. Taiwan Inst. Chem. Eng.*, 2016, **63**, 39–45.
199 R. Ponnusamy, R. Venkatesan, M. Kandasamy, B. Chakraborty and C. S. Rout, *Appl. Surf. Sci.*, 2019, **487**, 1033–1042.

200 C. Guo, H. Li, X. Zhang, H. Huo and C. Xu, *Sens. Actuators, B*, 2015, **206**, 407–414.
201 M. Li, J. Yang, M. Lu, Y. Zhang and X. Bo, *J. Colloid Interface Sci.*, 2019, **555**, 449–459.
202 L. Parashuram, S. Sreenivasa, S. Akshatha, V. Udayakumar and S. Sandeep kumar, *Food Chem.*, 2019, **300**, 125178.
203 R. Chung, A. Wang, Q. Liao and K. Chuang, *Nanomaterials*, 2017, **7**, 36.
204 J. H. Shim, A. Cha, Y. Lee and C. Lee, *Electroanalysis*, 2011, **23**, 2057–2062.
205 S. Liu, J. Tian, L. Wang, Y. Luo and X. Sun, *RSC Adv.*, 2012, **2**, 411–413.
206 M. N. Karim, S. R. Anderson, S. Singh, R. Ramanathan and V. Bansal, *Biosens. Bioelectron.*, 2018, **110**, 8–15.
207 S. Liu, J. Tian, L. Wang, Y. Zhang, Y. Luo, H. Li, A. M. Asiri, A. O. Al-Youbi and X. Sun, *ChemPlusChem*, 2012, **77**, 541–544.
208 Y. Zhang, J. Tian, S. Liu, L. Wang, X. Qin, W. Lu, G. Chang, Y. Luo, A. M. Asiri, A. O. Al-Youbi and X. Sun, *Analyst*, 2012, **137**, 1325–1328.
209 M.-S. Steiner, A. Duerkop and O. S. Wolfbeis, *Chem. Soc. Rev.*, 2011, **40**, 4805–4839.
210 Y. Cui, F. Chen and X.-B. Yin, *Biosens. Bioelectron.*, 2019, **135**, 208–215.
211 L. Wang, W. Zhu, W. Lu, X. Qin and X. Xu, *Biosens. Bioelectron.*, 2018, **111**, 41–46.
212 J. Luo, P. Luo, M. Xie, K. Du, B. Zhao, F. Pan, P. Fan, F. Zeng, D. Zhang, Z. Zheng and G. Liang, *Biosens. Bioelectron.*, 2013, **49**, 512–518.
213 S. Chaiyo, E. Mehmeti, W. Siangproh, T. L. Hoang, H. P. Nguyen, O. Chailapakul and K. Kalcher, *Biosens. Bioelectron.*, 2018, **102**, 113–120.
214 D.-M. Kim, J.-M. Moon, W.-C. Lee, J.-H. Yoon, C. S. Choi and Y.-B. Shim, *Biosens. Bioelectron.*, 2017, **91**, 276–283.
215 E. V. Karpova, E. V. Shcherbacheva, A. A. Galushin, D. V. Vokhmyanina, E. E. Karyakina and A. A. Karyakin, *Anal. Chem.*, 2019, **91**, 3778–3783.
216 Y. X. Wen, S. G. Liu, B. X. Tao, H. Q. Luo and N. B. Li, *Sens. Actuators, B*, 2020, **304**, 127279.
217 S. Bag, A. Baksi, S. H. Nandam, D. Wang, X. Ye, J. Ghosh, T. Pradeep and H. Hahn, *ACS Nano*, 2020, **14**, 5543–5552.
218 Y. J. Hong, H. Lee, J. Kim, M. Lee, H. J. Choi, T. Hyeon and D. H. Kim, *Adv. Funct. Mater.*, 2018, **28**, 1805754.